

---

# WHEN STYLE SIMILARITY SCORES FAIL: DIAGNOSING RAW CSD COSINE IN ARTIST-STYLE EVALUATION

---

A PREPRINT

✉ Jörg Frochte

Bochum University of Applied Sciences  
joerg.frochte@hs-bochum.de

## ABSTRACT

Raw cosine in the 768-dimensional output space of the Contrastive Style Descriptor (CSD) [14] is now widely read as an *absolute*, calibrated style-fidelity score for text-to-image and style-imitation evaluation. We introduce the *discrimination gap*, a corpus-internal, prototype-free and threshold-free diagnostic that tests whether contrastive style cosines admit an absolute same-versus-different interpretation on a candidate artist corpus. On a 1799-artwork, 91-artist public-domain corpus, raw CSD cosine yields negative point-estimate gaps for 23/91 artists at the pairwise level (2/91 robust under bootstrap) and for 15/91 in the aggregated-pool scoring regime style-fidelity evaluations typically use. CSLS readout [3] on the frozen backbone reduces the aggregated negative-gap count to 4/91; combined with positional-embedding interpolation to 336 pixels it raises unsupervised pair-verification AUC from 0.883 to 0.905 across 25 artist-disjoint splits. We refer to this diagnostic-driven readout protocol on the frozen backbone (CSLS as default, pos-interp 336 as the stronger optional setting) as CSD+, not a new encoder. A cross-backbone check on CLIP-ViT-L/14, SigLIP-large and DINOv2-Large reproduces the same shared-tradition failure pattern, providing evidence that the residual reflects a shared limitation of the four backbones we tested rather than a CSD-specific artefact. Practical implication: before reporting CSD cosine as an absolute style-fidelity score, run the diagnostic on the candidate corpus; CSLS is the minimal correction when it fails.

**Keywords** text-to-image style evaluation · contrastive style descriptor (CSD) · discrimination gap · CSLS · zero-training readout · pretrained vision encoders · hubness · validity diagnostic

## 1 Introduction

Diffusion-based image generators are increasingly evaluated for their ability to imitate, or to refrain from imitating, an artist’s style. The de-facto numerical proxy for style itself has become the Contrastive Style Descriptor (CSD) of Somepalli et al. [14], a ViT-L/14 fine-tuned on WikiArt artist labels. Cosine similarity in CSD’s 768-dimensional output space is now widely cited as an absolute, calibrated measure of stylistic distance: it is averaged over a fixed pool of an artist’s authentic works, treated as a scalar style-fidelity score, and read as evidence that one model produces “more faithful” renderings than another at the level of one or two percentage points. The central question of this paper is not whether CSD is useful as a retrieval embedding, but when its raw cosine can legitimately be interpreted as an absolute style-fidelity score on a given corpus, and what to do when it cannot. On a 1799-artwork, 91-artist public-domain corpus (curated by per-image VLM audit, see §3) we find that for 23 of 91 artists the within-class median cosine is *lower* than the highest cross-class median to some other artist; in the practical aggregated-pool scoring regime the negative-gap count drops to 15 but does not vanish. Two zero-training levers (CSLS readout and positional-embedding interpolation to 336 pixels) raise unsupervised pair-verification AUC from  $0.883 \pm 0.016$  to  $0.905 \pm 0.016$  across 25 artist-disjoint splits, combining sub-additively. The same shared-tradition pattern appears on CLIP-ViT-L/14, SigLIP-large and DINOv2-Large, providing evidence that the residual is a shared limitation of the backbones we tested rather than a CSD-specific quirk.

The original CSD work validates a specific operationalisation of the metric, and the practice we examine extends it. Somapalli et al. [14] report mean-average-precision and recall-at- $k$  on WikiArt’s 1119-artist retrieval benchmark and frame CSD as a tool for retrieving stylistically related images from a reference pool. Their 0.5 and 0.8 similarity thresholds are explicitly hypothesised, in the authors’ own phrasing, for one specific binary task (deciding whether an artist is in Stable Diffusion 2.1’s training corpus), and are computed against per-artist prototype vectors built from many SD generations rather than against individual reference images. Their Section 6.1 confusion analysis is reported at the level of art movements, with the explicit observation that the metric struggles to separate artists working in the same tradition. Downstream evaluations often operationalise raw cosine in a stronger way than the original validation supports (as a per-image, calibrated, absolute style-distance score read off from a single artwork, rather than as a retrieval-pool similarity measured against many reference images), and we ask under what corpus conditions that stronger reading is warranted.

Concretely, this paper makes four contributions. First, we introduce the discrimination gap  $g_k = w_k - c_k$ , a corpus-internal, prototype-free, threshold-free diagnostic that tests, for any artist  $k$  on any candidate corpus, whether raw pairwise cosine is in a usable regime as an absolute same-versus-different score. To our knowledge, this is the first corpus-internal diagnostic specifically aimed at testing absolute-score interpretability in artist-level style evaluation. Second, we use this diagnostic to surface a systematic failure mode: on our 91-artist corpus 23/91 artists have a negative point-estimate gap at the pairwise level (2/91 robust under bootstrap) and 15/91 under the aggregated pool-scoring regime that T2I style-fidelity evaluations typically use, with the worst-other artist for each mapping onto a known art-historical tradition in every case. Third, we provide a diagnostic-driven readout correction: CSD+ is a readout protocol on the frozen CSD backbone, not a new encoder. CSLS readout [3] on vanilla 224 is the default and reduces the aggregated negative-gap count from 15/91 to 4/91 at no embedding-time overhead; combining CSLS with positional-embedding interpolation [8] to 336 raises pair-verification AUC to  $0.905 \pm 0.016$  at  $\approx 2.25\times$  embedding cost. Both levers are individually well known; what is new is the diagnostic-driven application of CSLS to visual style discrimination and the sub-additive interaction we measure. Fourth, we show that the residual failures replicate across the backbones we tested: the few artists that survive every zero-training correction reproduce the same shared-tradition failure on CLIP-ViT-L/14, SigLIP-large and DINOv2-Large, providing evidence that the residual is common to the four vision embedding backbones we tested rather than a CSD-specific artefact. §9 summarises the practitioner-oriented recipe choice as a corollary.

## 2 Background and Operational Setting

CSD sits within a longer line of work on quantifying stylistic similarity. Classical neural style transfer [5] uses VGG-Gram matrices as the canonical perceptual baseline; the diffusion-evaluation literature subsequently moved to large-scale pretrained encoders, principally CLIP [9] and DINOv2 [8], neither of which carries explicit style supervision. CSD [14] is the first widely used metric to add explicit artist-level supervision through a multi-label contrastive objective on WikiArt artist labels. Recent text-to-image work has adopted CSD cosine in two distinct roles. As a style-fidelity *evaluation column* alongside CLIP-I and DINO scores in style-personalisation, content/style disentanglement and continual-personalisation benchmarks: Magic Insert [12] reports CSD as a style-fidelity score in its main comparison; UnZipLoRA [6] uses both *Style-align (CSD)* and *Subject-align (CSD)* as the more sensitive separation metric over CLIP/DINO; the continual personalisation study of Staniszewski et al. [15] reports CSD as the style-side Average Score and Average Forgetting metric. As a *feature extractor inside the sampler*, where CSD-feature differences against a reference provide a guidance gradient (InstantStyle-Plus [16]) or enter a stochastic-optimal-control terminal cost (RB-Modulation [11]). The CSD authors themselves use thresholds of 0.5 and 0.8 against per-artist prototypes for the binary “is this artist in SD-2.1’s corpus?” check. The evaluation-column rows are the practice this paper interrogates: they read CSD cosine as an absolute style-fidelity score that is comparable across artists, which the discrimination diagnostic of §4 reads as warranted only when the per-artist gap on the candidate corpus is positive.

The diagnostic of §4 surfaces a pattern (a small number of artist clusters appearing as universal nearest neighbours) with a long history in the embedding-geometry literature. Radovanović et al. [10] establish that “hubs” are an inherent property of high-dimensional data and link the phenomenon to intrinsic dimensionality. Cross-domain Similarity Local Scaling (CSLS) [3] was introduced as an explicit hubness correction in bilingual lexicon induction. We carry it across to pool-based artist discrimination and show that the same construction that suppresses lexical hubs also suppresses the median-cross hubness our diagnostic exposes (the Goya pattern in §5). Mu and Viswanath [7] note that contrastive embeddings tend to have a non-zero common mean and a few dominating directions and propose simple post-processing recipes; the score-level intervention of §5 (CSLS) lives in that family conceptually but operates on the local-density readout directly, rather than on the embedding vectors. App. B reports centering, all-but-the-top and PCA-whitening as embedding-level alternatives.

This paper studies the two downstream uses where raw CSD cosine is most often read as an absolute score. *Style-fidelity scoring* (mean cosine to an artist’s anchor pool) carries the risk of false absolute calibration when the per-artist gap on the candidate corpus is not positive; §4 addresses this via the discrimination gap. *Pair verification* (pair cosine between two candidates) carries the risk that a scalar cosine discards vector information a learned head could exploit; §6 addresses this via the zero-training CSD+ recipe. Nearest-neighbour retrieval (validated by Somepalli et al. [14]) and closed-set discrimination against a fixed candidate pool are out of scope.

### 3 Corpus and Embeddings

We anchor the artist set on the 400-artist list released with the CSD code repository, so that any empirical claim is anchored on artists the original authors themselves identified as relevant to the study of style. The list contains substantial duplication (the same artist appears repeatedly under different name spellings); after canonical-name deduplication, 367 distinct artists remain. The list is heavily Western-canonical; to avoid making all our findings about Western art alone, we add fourteen non-Western artists spanning Edo-period Japan, Ming-dynasty China and modern Chinese ink, Joseon-dynasty Korea, Persian and Mughal miniature, Indian Academic realism, and Mexican popular print. To fill specific gaps in the original CSD list (Spanish Baroque, French Romanticism, American Tonalism, Cubism, Naive art, Early-Renaissance Italian painting, Symbolist and French-Academic) we further add a small number of artists per tradition; the augmentations and the full retained-artist list are in App. A. For each canonical name we attempt a public-domain artwork fetch from Wikimedia Commons via the Wikidata-resolved Commons category. The fetched candidates pass through a two-stage audit (regex filter, language-model attribution judge, and per-image vision–language content vetting) that excludes attributional and off-topic retrieval noise; details and full reject categories are in App. A. After audit, 91 artists remain in the working corpus with 1799 retained anchors (mean 19.8 per artist, range 11–27); per-anchor attribution labels (*master, workshop, school, after, attributed*) are carried through to the embedding NPZ as a side channel. By style-recognition standards this is a modest corpus and we treat it as such: aggregate claims are reported with explicit cluster, movement and worst-neighbour controls (§§4, 6) rather than as single-number averages, the verification analysis is replicated across 25 artist-disjoint splits, and the attribution side-channel acts as an independent check that the shared-tradition difficulty we report is not an artefact of mis-attributed workshop pieces. Movement-and-tradition labels are author-curated from a 47-label vocabulary covering the major Western traditions and the non-Western categories the corpus addition introduces. Full fetcher, audit and labelling details, including the fetched-but-rejected artists, are in App. A.

For each artwork we resize the shortest side to 512 pixels, take a centre crop, and pass the result through the vendored CSD ViT-L checkpoint at the authors’ standard  $224 \times 224$  input; the 768-dimensional output is  $L^2$ -normalised. All downstream analysis operates on these 1799 vectors. We use the standard CSD pipeline so that the diagnostic of §4 reports on CSD as the community uses it; §6 examines alternative input variants when verification, not the diagnostic, is the goal.

### 4 Diagnostic: When Raw CSD Cosine Fails

The discrimination gap defined in this section is the minimal corpus-internal condition under which raw cosine on CSD-768 is interpretable as an absolute same-versus-different score: it is not an auxiliary statistic but the test that decides whether the absolute reading the downstream literature applies to CSD cosine is even defensible on the candidate corpus. For each artist  $k$  we define two summary statistics over the corpus’s pairwise cosines. The within-class median  $w_k$  is the median of cosines among artist  $k$ ’s own artworks, taken over off-diagonal pairs so that self-similarity does not bias the result upward. The cross-class statistic  $c_k$  is the maximum, over every other artist  $j \neq k$ , of the median cosine between  $k$ ’s anchors and  $j$ ’s anchors. The discrimination gap is  $g_k = w_k - c_k$ . A positive gap means an arbitrary anchor of  $k$  sits, in median, closer to its own artist’s pool than to any other artist’s pool, which is the minimal condition under which raw pairwise cosine, read as an absolute same-versus-different score, is order-consistent on  $k$ . A negative gap means there exists at least one other artist  $j$  whose median pairwise cosine to  $k$ ’s anchors exceeds  $k$ ’s within-class median, so that the raw-cosine ordering, read as an absolute score, is median-inverted for  $k$  against  $j$ . The diagnostic does not say that no cosine-based readout can recover the discrimination, only that the absolute interpretation of raw pairwise cosine is unsafe; CSLS-style local-density readouts (§5) operate on the same cosine values and recover most of the discrimination. The gap is defined entirely on the corpus we measure it on; it does not depend on a similarity threshold or on prototype construction. Fig. 1 illustrates the two cases.

Computed across the 91 artists, the gap is negative for 23 of them (25.3%). Forty-two artists (46.2%) have a gap below 0.05, a threshold at which within-class and cross-class medians are within sampling variability of each other. Only ten artists (11.0%) reach a gap of at least 0.15, the regime we describe as cleanly separated. The aggregate negative-gap count is robust to anchor-pool sampling: across 100 bootstrap resamples (drawn with replacement, per artist, at the

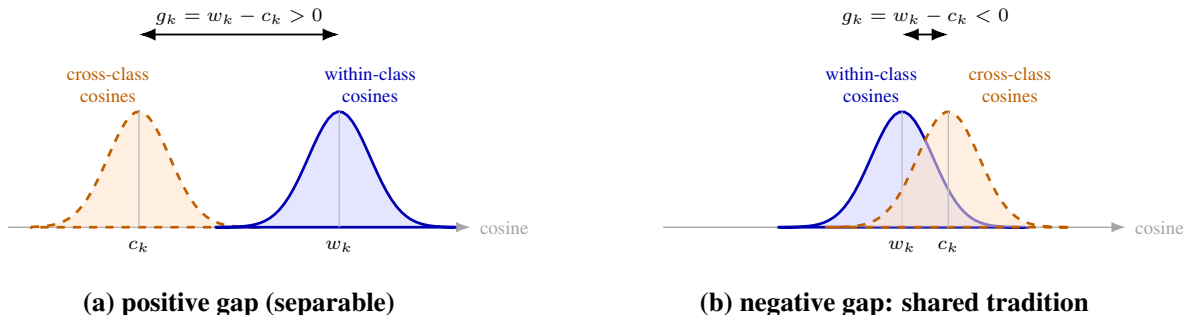


Figure 1: Discrimination-gap intuition. (a) Within-class cosines (blue) well separated from the closest cross-class cosines (orange): gap positive, raw cosine usable as a same-versus-different score on this corpus. (b) Shared-tradition pair, populations overlap or invert: gap negative, raw cosine misorders the pair.

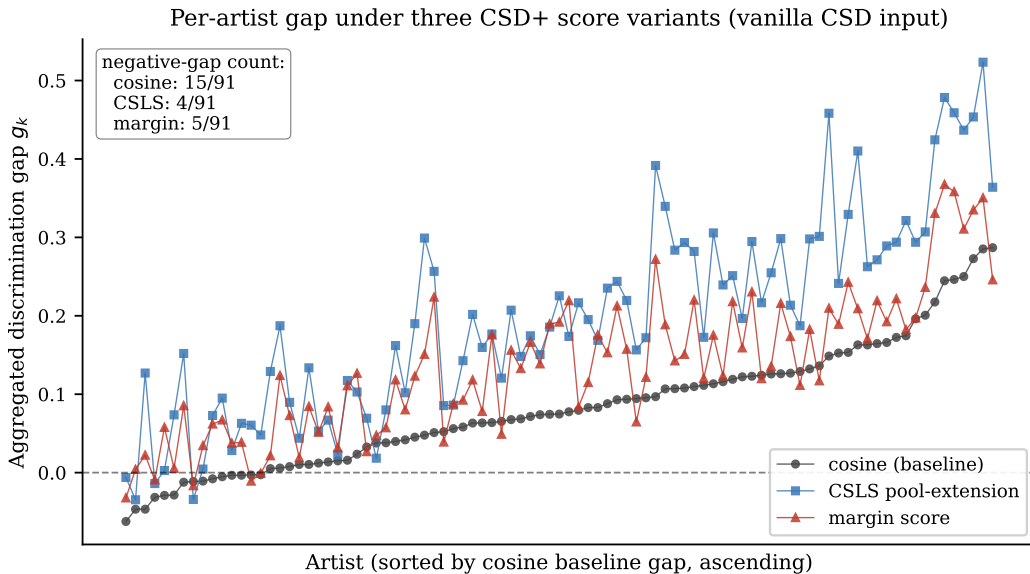


Figure 2: Per-artist aggregated gap across 91 artists, sorted ascending by the cosine baseline; three CSD+ variants overlaid (cosine, CSLS, margin). Markers below the dashed zero line are negative-gap artists; inset: per-variant counts.

same per-artist size) the count is  $21.9 \pm 2.7$ , range [16, 28]. The aggregate count and the per-artist robustness are distinct estimands, and we report both. At the per-artist level, the 95% bootstrap CI of  $g_k$  remains entirely below zero for only 2 of the 23 negative-gap artists (Delacroix, Kyōsai); the other 21 have CIs that cross zero, reflecting small per-artist anchor counts ( $n_k \in [11, 25]$  for most). The shared-tradition pattern is therefore robust at the population level (the count of negative gaps is reproducible) but for many individual artists near zero the classification should be read as *ambiguous* rather than categorically failed; the worst-case pairs that the rest of the paper emphasises are those whose CIs lie clearly below zero or whose shared-tradition partner is independently identifiable. Per-artist CIs are tabulated in App. A, Tab. 7; the same appendix shows that the worst-other identity for each negative-gap artist is stable in 100% of random 70-artist subsamples (Tab. 8), so the pairs are geometrically intrinsic rather than artefacts of the specific artist set. Fig. 2 plots the full sorted distribution; Tab. 1 lists the fifteen worst-case artists.

Reading down Tab. 1, the identity of each artist’s nearest non-self neighbour repeatedly maps onto a known art-historical tradition. Representative pairs across Western traditions: Raffaello/Mantegna at gap  $-0.085$  (Italian Renaissance), Delacroix/Goya at  $-0.083$  (European Romanticism), Doré/Goya at  $-0.040$  (Romantic-illustrative), Leighton/Waterhouse at  $-0.040$  (Victorian Academic / Pre-Raphaelite), and Levitan/Shishkin at  $-0.030$  (Russian Realist landscape). The non-Western side generalises the pattern within Edo-period Japanese traditions: Hasegawa Tōhaku and Tōshūsai Sharaku at  $-0.074$ , and Kawanabe Kyōsai and Sharaku at  $-0.049$ . Of the twenty-three negative-gap artists, every single one can be paired with a known art-historical neighbour on these grounds. A particular role is

Artist	$n$	$w_k$	$c_k$ (max)	Worst other	Gap $g_k$
Mikhail Vrubel	14	+0.149	+0.247	Louis Comfort Tiffany	-0.098
Raffaello Sanzio	18	+0.335	+0.420	Andrea Mantegna	-0.085
Eugène Delacroix	23	+0.372	+0.455	Francisco Goya	-0.083
Hasegawa Tōhaku	12	+0.420	+0.494	Tōshūsai Sharaku	-0.074
Sandro Botticelli	15	+0.318	+0.389	Andrea Mantegna	-0.071
Ivan Bilibin	23	+0.258	+0.313	José Guadalupe Posada	-0.055
Kawanabe Kyōsai	20	+0.479	+0.527	Tōshūsai Sharaku	-0.049
Gustave Doré	23	+0.277	+0.317	Francisco Goya	-0.040
Frederic Leighton	19	+0.253	+0.293	John William Waterhouse	-0.040
Maxfield Parrish	25	+0.339	+0.379	Kitagawa Utamaro	-0.039
Isaac Levitan	20	+0.289	+0.319	Ivan Shishkin	-0.030
Albert Aublet	18	+0.228	+0.257	Francisco Goya	-0.029
Diego Velázquez	17	+0.385	+0.409	Georges de La Tour	-0.024
Itō Jakuchū	11	+0.463	+0.482	Tōshūsai Sharaku	-0.019
Gustav Klimt	20	+0.283	+0.301	Odilon Redon	-0.019

Table 1: Top-15 artists by most negative discrimination gap; definitions in §4. Of 91 artists, 23 have a negative gap.

played by Francisco Goya, who appears as the worst other for several artists: Goya’s own within-class cohesion is the highest in the corpus at  $w_k = 0.780$ , his works form the densest cluster in CSD’s output space, and that density positions him close, in cosine terms, to several tonal-landscape and Romantic artists whose own clusters are more diffuse, a manifestation of the hubness phenomenon [10] that motivates the hubness-aware CSLS readout of §5. App. A (Fig. 5) renders one of the shared-tradition pairs concretely with four PD-Art exemplars from Levitan and Shishkin.

The pattern across all twenty-three artists is consistent with a structural account that follows from how CSD was trained. The contrastive objective pulls works of the same WikiArt artist together and pushes works of different artists apart, but has no signal that distinguishes “different artists in the same tradition” from “different artists with unrelated styles”. When two artists in WikiArt produce landscapes with similar palette, atmospheric perspective and compositional tropes, the push gradient is small and easily overwhelmed by the same-artist pull, leaving the resulting clusters near-overlapping, which is precisely what we measure. Somepalli et al. [14] themselves anticipate this in their Section 6.1 discussion of impressionist landscape painters and of Picasso versus Braque; what our corpus adds is the demonstration that the phenomenon is not confined to a few annotated movements or to Western art alone: the same pattern recurs across every shared tradition in our corpus represented by at least three artists, at an aggregate magnitude (more than a quarter of artists affected) that makes uncritical use of CSD cosine as an absolute style-fidelity score unsafe across an arbitrary artist set.

## 5 CSD+ Readouts for Practical Evaluation

We do not propose a new style encoder. CSD+ is a diagnostic-driven readout protocol on the frozen CSD backbone: use raw cosine only when the diagnostic of §4 validates the absolute-score interpretation; otherwise use CSLS as the minimal zero-training correction, optionally combined with 336-pixel positional interpolation when additional embedding cost is acceptable. This section quantifies the correction; §7 characterises what remains.

The diagnostic of §4 measures pairwise medians; in practice, downstream evaluations aggregate cosine across an artist’s anchor pool and quote the result as a style-fidelity score. We therefore lift the diagnostic to the per-query aggregated score  $s(x, A) = \frac{1}{|A|} \sum_{a \in A} \cos(x, a)$ , the quantity LoRA-evaluation pipelines actually compute when they grade a generation  $x$  against an artist’s anchor pool  $A$ . Within- and cross-class statistics, and the discrimination gap derived from them, are defined on  $s$  in the obvious way; for an anchor  $x \in A$ , the within-class score is computed leave-one-out (the mean runs over  $A \setminus \{x\}$ ) so that  $\cos(x, x) = 1$  does not artificially inflate the within-class side of the gap. Under raw cosine, 15 of the 91 artists in our corpus exhibit a negative aggregated gap; the number is lower than the 23 of the pair-level diagnostic because aggregation averages out some per-pair variance, but the underlying phenomenon is the same.

The question this section answers is which zero-training readout reliably brings the negative-gap count down. The recipe we recommend is Cross-domain Similarity Local Scaling (CSLS) [3]. CSLS targets the absolute-score interpretation directly: it removes the inflation of cosine values in regions of the embedding where many points are mutually close, which the diagnostic identifies as the structural cause of the negative-gap pattern. With  $r_k(x) = \frac{1}{k} \sum_{y \in N_k(x)} \langle x, y \rangle$  denoting the mean cosine of  $x$  to its  $k$  nearest neighbours,  $\text{CSLS}(x, A) = 2s(x, A) - r_k(x) - \frac{1}{|A|} \sum_{a \in A} r_k(a)$  is the

doubly-locally-centred analogue of  $s$ . Empirically (Table 2, vanilla 224-pixel CSD) CSLS reduces the negative-gap count from 15/91 to 4/91; the residuals are shared-tradition pairs that §7 characterises as representational rather than readout limits. Goya is the canonical median-cross hub the construction was meant to suppress: under raw cosine he ranks 41<sup>st</sup> of 91 in hub-inclusion (0.056); under CSLS he drops to rank 91 with hub-inclusion 0.017, a 70% reduction. We use  $k = 15$  [3], below the median per-artist anchor count of 20; counts and AUC are stable across  $k \in \{5, 10, 15, 20, 50\}$  (App. B, Tab. 14). The reference pool over which local densities are computed is the candidate evaluation corpus itself; we treat CSLS as a readout for the pool-based benchmark setting in which CSD cosine is reported, not as a claim about isolated single-query deployment without a reference corpus. Pool-sensitivity matches raw cosine: the worst-other identity for each CSLS-neg-gap artist is preserved in 100% of random 70-artist subsamples (App. A, Tab. 9).

For comparison and as a negative control, the per-cohort z-score  $z(x, A) = (s(x, A) - \mu_A) / \sigma_A$  rescales each artist’s score against its own oeuvre’s spread, addressing within-class median variation between 0.247 (Mikhail Vrubel) and 0.807 (Tōshūsai Sharaku). It is a *per-target* rescaling that depends on  $A$ ’s pool but not on any competing class and therefore has no systematic dependence on the cross-class geometry that produced the negative gaps; the empirical result in Tab. 2 confirms that no negative gaps flip on our corpus. Cohort- $z$  is the right tool for cross-artist score *comparability* (“this generation scores at the 70th percentile of Goya’s own oeuvre”), not for the absolute-score interpretation our diagnostic flags.

Method	# neg gap	median gap
Plain cosine $s(x, A)$ (baseline)	15	+0.075
CSLS pool-extension	4	+0.187
Cohort z-score per artist	15	+0.516
Margin score $m(x, A)$	5	+0.127

Table 2: Score-level variants on vanilla 224-pixel CSD input; counts and medians are over the 91 artists and deterministic on the full corpus. Pair-verification AUCs for cosine and CSLS are in Tab. 4; cohort- $z$  and margin are diagnostic-side only.

A complementary axis of intervention modifies CSD’s input pipeline rather than its readout, again without retraining the backbone. CSD’s ViT-L/14 has a fixed  $16 \times 16$  patch grid corresponding to its trained  $224 \times 224$  input. Bilinear interpolation of the trained positional embeddings to a  $24 \times 24$  grid permits inference at  $336 \times 336$  on the same backbone weights, raising the effective spatial resolution by  $1.5\times$ . The trick is well-established for ViT-based image encoders [8]; we apply it as a single forward pass per image at the higher resolution, at the cost of about  $2.25\times$  more patches per forward pass. A scale ablation across  $\{224, 280, 336, 392, 448\}$  in App. B shows that the discrimination diagnostic improves monotonically up to  $\approx 280$  and saturates by 336, while verification AUC peaks at 280–336 and degrades beyond 336. We adopt 336 as the operational recipe because it sits at the saturating shoulder where verification has not yet started to degrade and the discrimination diagnostic is at its plateau. Multi-crop aggregation (five  $224 \times 224$  crops from a  $256 \times 256$  base) gives a smaller verification gain than pos-interp 336 on every cell of the verification grid: read as a Monte-Carlo estimator, multi-crop is a variance reduction at fixed bias, whereas pos-interp removes the truncation bias outright. Full derivation and the multi-crop ablation are in App. B.

The sub-additive interaction between CSLS and pos-interp (+0.017 and +0.012 in isolation, +0.022 combined) gives an empirical error-structure reading rather than a formal decomposition. The two interventions do not correct independent error components. Pos-interp recovers spatial evidence that the 224-pixel input truncates, whereas CSLS suppresses local-density-induced score inflation. The overlap suggests that part of the apparent hubness is induced or amplified by the same missing spatial evidence that higher-resolution inference partially restores; CSLS on top of pos-interp therefore corrects what survives the spatial-evidence recovery.

CSLS was originally introduced for cross-lingual lexicon induction in word embedding spaces. Its unmodified transfer to artist-style discrimination provides evidence that hubness is a modality-spanning failure mode of high-dimensional contrastive embeddings rather than a peculiarity of language embeddings.

Empirically, pos-interp 336 alone raises cosine AUC from 0.883 to 0.895, CSLS alone raises it to 0.900, and their combination reaches  $0.905 \pm 0.016$  across 25 splits (§6; Tab. 3 reports the discrimination-side grid). CSLS on vanilla 224 reaches the lowest aggregated negative-gap count of the three recommended input pipelines (4/91 vs 5/91 for CSLS+336, Tab. 3) and is the default; CSLS+336 is the stronger setting for pair-verification AUC at  $\approx 2.25\times$  embedding cost.

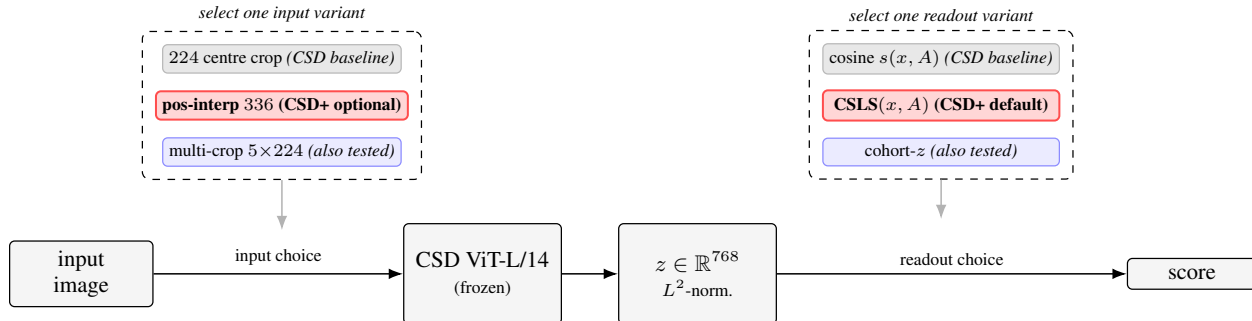


Figure 3: CSD+ along the unchanged CSD pipeline. Two choice points are exposed: input variant (before the encoder) and readout variant (after the embedding). Grey: CSD baseline (centre-crop 224 + raw cosine). Red: recommended CSD+ recipes (CSLS on vanilla 224 as default, pos-interp 336 as the stronger setting for verification AUC on the input side). Blue: comparison variants (multi-crop and cohort- $z$ ).

Score variant	vanilla 224	multi-crop 5x224	pos-interp 336
cosine	15	11	11
CSLS	4	5	5
margin	5	4	5
cohort- $z$	15	11	11

Table 3: CSD+ grid (compact). Each cell is the number of artists (of 91) with negative aggregated discrimination gap under the row’s score-level variant and the column’s input pipeline. The full  $6 \times 4$  matrix (all five resolutions plus multi-crop, with median-gap values) is in App. B, Tab. 10.

## 6 Input Resolution and Pair Verification

A separate operational question, motivated by authentication and style-attribution, is whether two given artworks were created by the same artist: a verification task in the sense familiar from face recognition [13], with the test condition that the verifier never sees the test artists during training. We construct the task from the 91-artist corpus by splitting artists (not artworks) into 73 training artists and 18 held-out test artists; from the test pool we sample 1500 same-artist and 1500 different-artist pairs per split. We report results across 25 random artist-disjoint splits and quote AUC as mean  $\pm$  standard deviation, with the per-split paired comparisons that constitute the actual evidence for or against each method.

Three families of methods are compared on the same 25 splits. Raw cosine on 768-dimensional CSD output, applied without training, is the unsupervised baseline. A pair-feature logistic regression on  $\phi(a, b) = \frac{1}{2} \left[ |a - b| + |a \odot b| \right] \in \mathbb{R}^{2304}$ , trained on the 73 training artists, is the supervised baseline; the three blocks expose absolute disagreement, multiplicative interaction, and pair location to a linear head, following established sentence-pair encoding practice [2]. A learned Mahalanobis distance parametrised through its Cholesky factor regressed below cosine in our experiments (AUC 0.873 on a single fixed split, versus 0.915 for cosine on the same split), which we report as a methodological note: directly learning a positive-definite metric on pair-difference vectors does not generalise to held-out artists in our setting. The simpler pair-feature logistic regression avoids that overfit.

Method	AUC mean $\pm$ std	AUC range	EER mean
Cosine on vanilla CSD (224)	0.883 $\pm$ 0.016	[0.848, 0.912]	0.197
CSLS on vanilla CSD (224)	0.900 $\pm$ 0.016	[0.870, 0.930]	0.182
Cosine on pos-interp 336 (CSD+)	0.895 $\pm$ 0.016	[0.858, 0.929]	0.183
CSLS on pos-interp 336 (CSD+)	0.905 $\pm$ 0.016	[0.874, 0.939]	0.175
Pair-logreg on vanilla CSD (224)	0.917 $\pm$ 0.018	[0.878, 0.952]	0.163
Pair-logreg on pos-interp 336	0.917 $\pm$ 0.017	[0.874, 0.951]	0.165

Table 4: Verification AUC across 25 random artist-disjoint splits ( $n_{\text{train}} = 73$ ,  $n_{\text{test}} = 18$ ). Paired split comparisons (X/25-wins) are in App. B, Tab. 12.

Tab. 4 reports the 25-split AUCs. Paired 95% CIs (App. B, Tab. 12) exclude zero with margin:  $+0.017 [+0.014, +0.020]$  for CSLS,  $+0.012 [+0.010, +0.014]$  for pos-interp 336, and  $+0.022 [+0.019, +0.025]$  combined. The aggregate aver-

ages over easy and hard pairs; the practical impact concentrates where the diagnostic flags trouble: on Sharaku/Kyōsai, CSLS lifts pair-bidir of Kyōsai LoRA generations from 12% to 78% (§8), so a “0.42 vs 0.41” style-fidelity ranking is qualitatively unchanged on positive-gap artists but can flip on flagged negative-gap pairs. Input resolution and CSLS readout are partially overlapping zero-training levers; the combined recipe reaches  $0.905 \pm 0.016$  but only sub-additively. Operationally, scalar cosine on vanilla 224 underuses CSD in two ways (truncated spatial evidence and a locally density-biased readout); either lever recovers a substantial fraction of the gap. CSLS at 224 is the better cost-benefit point; CSLS+336 wins only when the  $\approx 2.25\times$  embedding cost is justified.

The headline AUCs are reported on negatives sampled uniformly at random from the held-out artist pool, so a non-trivial fraction of negative pairs are kunsthistorically far apart (a Hokusai versus a Monet, a Hudson River School landscape versus an Edo woodblock); these are pairs the diagnostic in §4 already separates by a wide margin. To probe the regime that the diagnostic flags as the actually difficult one, we re-evaluate the same 25 splits under three additional negative samplers and report results in App. B, Tab. 13. The *same-movement* regime conditions on the author-curated movement labels of §3 and pairs different-artist negatives within the same movement (Levitan vs Shishkin within Russian Realism, Leighton vs Godward within Victorian Academic, Hiroshige vs Utamaro within Edo-period Japan). The *worst-neighbour* regime is the more stringent per-split version: for each anchor of test artist  $k$ , the negative is drawn from  $B(k) = \arg \max_{j \in \text{test}, j \neq k} c_{k,j}$ , where  $c_{k,j}$  is the median cross-pair cosine on the full 91-artist corpus, so each anchor is paired with its hardest available counter-class. The *positive-gap control* restricts both pos and neg to test artists with full-corpus discrimination gap  $g_k > 0.05$  (roughly the upper half of the corpus), where raw cosine should be uncontroversially separating. Across all three methods, AUC drops by 0.17–0.19 from the random to the worst-neighbour regime, and rises by 0.04–0.05 in the positive-gap control. The pair-logreg classifier loses most of its random-regime advantage under worst-neighbour negatives ( $0.750 \pm 0.029$  vs  $0.738 \pm 0.022$  for CSLS, a  $+0.012$  margin versus  $+0.012$  in the random regime); the supervised head learns generic same-artist-vs-not-same-artist discrimination, not the within-tradition fibre coordinate that the diagnostic identifies as the hard problem. The same-movement regime is essentially indistinguishable from the random regime under the strict corpus ( $0.882 \pm 0.019$  vs  $0.882 \pm 0.014$  for cosine, both under the regime-specific sampling of App. B, Tab. 13), reflecting that the audit removes both photographs-of-artworks and museum-context shots that previously inflated within-movement overlap; the worst-neighbour regime is the stable per-split test of within-tradition difficulty. Read against §4, this is the verification-side reading of the same negative-gap finding: the AUC headline does not collapse to chance, but the within-tradition difficulty is a genuine 0.17–0.19 absolute AUC penalty, and CSLS narrows it by roughly the same fraction as it narrows the random-regime gap. Full per-regime AUC numbers are in App. B (Tab. 13).

When supervised training pairs are available, pair-feature logistic regression on the raw 768-dimensional CSD vector beats every cosine-style method (AUC  $0.917 \pm 0.018$  on vanilla 224, 25/25 splits) and is essentially unaffected by the input-pipeline upgrade. Block ablation, full numbers and discussion are in App. B.

The practical result is therefore: CSLS on vanilla 224 is the cheapest robust zero-training verification fix; CSLS+336 wins when the  $\approx 2.25\times$  embedding cost is acceptable; pair-feature logistic regression on the raw 768-d vector is the strongest recipe overall when supervised pairs are available.

Manifold-aware projections do not help verification: cosine on a UMAP-20D projection fit on training artists drops AUC by 0.112 on a reference split, and pair-logreg on UMAP-20D drops by 0.135. UMAP preserves  $k$ -NN topology, which on this corpus is dominated by tradition-level neighbourhoods rather than artist-level separation; the projection compresses precisely the dimension verification needs. Full table and the geometric reading are in App. C.

## 7 Residual Errors and the Shared-Tradition Limit

This section has two purposes: to show that the residual errors after the CSD+ recipes of §§5–6 persist across backbones, and to explain why they cluster around shared traditions. The recipes address what we have called readout artefacts and leave a small set of shared-tradition pairs that no zero-training intervention reaches: Frederic Leighton paired with John William Godward (Victorian Academic and Pre-Raphaelite, residual gap  $-0.009$  under pos-interp 336 + CSLS; Leighton’s raw §4 worst-other is Waterhouse at  $-0.040$ , not Godward), Diego Velázquez paired with Georges de La Tour (Spanish/French Baroque tenebrism), and Raffaello Sanzio paired with Andrea Mantegna (Italian Renaissance). The two readings below treat these as the same residual seen from different angles, not as separate findings.

The first reading is a cross-backbone replication on DINOv2-Large [8], CLIP-ViT-L/14 [9] and SigLIP-large [17]: three frozen ViT-L backbones spanning self-supervised, image-text contrastive and sigmoid-loss image-text training respectively. The question this answers is whether the residuals are CSD-specific or a property of the comparison backbones too. Embeddings are computed on the same 1799 artworks; the discrimination diagnostic and the 25-split verification sweep use the same seed family as §6. Two points read off Tab. 5. CSD, CLIP and SigLIP perform similarly on cosine verification (0.883, 0.873, 0.896 respectively, with SigLIP marginally above CSD); DINOv2 is significantly

backbone	discrimination			verification AUC	
	# neg (cos)	median gap	# neg (CSLS)	cosine	CSLS
CSD vanilla 224	15	+0.075	4	$0.883 \pm 0.016$	$0.900 \pm 0.016$
CLIP-ViT-L/14	16	+0.035	1	$0.873 \pm 0.020$	$0.909 \pm 0.019$
SigLIP-large	13	+0.045	2	$0.896 \pm 0.017$	$0.914 \pm 0.018$
DINOv2-Large	38	+0.007	19	$0.789 \pm 0.029$	$0.831 \pm 0.028$

Table 5: Cross-backbone comparison on the 91-artist corpus. The shared-tradition negative-gap pattern is present on all four backbones; CSLS lifts verification AUC by 0.02–0.04 across the family and reduces the negative-gap count to 1–19. The DINOv2 row isolates the role of text/artist supervision; §7 discusses.

worse at 0.789, showing that some explicit text or style supervision is needed to encode artist-level discrimination. Second, the shared-tradition failure mode holds on every backbone: 15, 16, 13 negative-gap artists for CSD, CLIP, SigLIP under cosine, and 38 for DINOv2, with the same artist clusters surfacing as worst neighbours across all four. CSLS lifts every backbone’s verification AUC by +0.02 to +0.04 and reduces the negative-gap count to 1–19, so the score-level recipe is backbone-agnostic; the residual it does not eliminate is consistent across CSD, CLIP, SigLIP and DINOv2.

The DINOv2 row also isolates the role of supervision. Self-supervised visual features capture broad perceptual and compositional structure but are less aligned with artist-level style discrimination than image-text- or artist-supervised embeddings; this shows up as a significantly lower cosine AUC (0.789 vs. 0.873–0.896) and a much higher negative-gap count (38 vs. 13–16). At the same time, the fact that CSD, CLIP and SigLIP share the same residual shared-tradition confusions indicates that supervision improves artist-level separability without eliminating intra-tradition overlap.

The second reading is unsupervised clustering, and it explains the *shape* of the residual rather than just its persistence. UMAP-20D followed by HDBSCAN on the raw 1799 vectors recovers 51 clusters at the canonical seed (averaging 68 across 10 seeds); the shared-tradition pairs the diagnostic flags reappear as cohesive clusters of their own: a Cubism cluster (Gris, Picabia, Gleizes), an Italian-Renaissance cluster (Mantegna, Botticelli, Raffaello), an East-Asian brush-painting cluster (Shen Zhou, Kyōsai, Tōhaku, Jakuchū), a Spanish-Baroque/Dutch-Golden-Age tenebrism cluster (La Tour, Vermeer, Velázquez, Zurbarán, Murillo) and a Pre-Raphaelite cluster (Rossetti, Bouguereau, De Morgan, Waterhouse, Leighton). The largest cluster (Hudson River School and adjacent landscape painting, 321 points) is the same pattern at corpus scale: the landscape family is grouped as one stylistic family, with no attempt to separate its individual artists, mirroring the Gifford/Church and Cole/Bierstadt negative-gap finding in §4. The residual errors after CSD+ are therefore not noise around a clean signal but real stylistic families that the embedding does not separate at the artist level. The HDBSCAN clustering is label-free, so this confirmation of the shared-tradition interpretation does not depend on the author-curated movement labels of §3. Full intrinsic-dimensionality estimate, clustering sweep across ten pipelines, and per-cluster compositions are in App. C.

## 8 T2I-Style-Eval Implications

We use T2I not as a separate benchmark but as a stress test of the diagnostic. The discrimination gap of §4 is defined on *original* artworks; if it is a genuine validity diagnostic, it should also predict when generated images can be evaluated by CSD-style scores. We test this on Flux-1 dev [1] as a representative current-generation flow-matching backbone.

We first prompt bare Flux-1 dev (no LoRA) with 22 neutral subjects  $\times$  3 seeds, formatted as "`<subject>`, art by `<artist>`", for 15 artists from the corpus, then CSD-embed each generation and ask whether the artist’s own anchor is the top-1 match across all 91 corpus classes. Three regimes emerge (Tab. 18 in App. D). Tier-1: the artist’s name token works as a style trigger and CSD localises it correctly: Sharaku 56% top-1 and La Tour 53% top-1 are the canonical examples. Tier-2: the prompt reaches the right *tradition* cluster but not the artist (Hokusai top-1 0% but top-5 14% in Edo-print; Church top-1 26% but top-5 88% in Hudson River School). Tier-3: bare prompting misses entirely: Van Gogh, Monet, Klimt, Leighton, Levitan all under 3% top-1. The implication is methodological: bare-prompted T2I cannot serve as the basis for CSD-style evaluation across an arbitrary 91-artist set; for most artists the bare prompt fails for reasons that have nothing to do with CSD itself.

A natural answer is to actively style-condition the generator. We LoRA-train Flux-1 dev on three pairs spanning the negative-gap spectrum: Sharaku/Kyōsai and Levitan/Shishkin (§4 raw worst-other pairs, gaps  $-0.049$  and  $-0.030$ ) and Leighton/Godward (§7 CSD+-residual at  $-0.009$ ), and on two positive-control artists whose bare-prompt behaviour falls in Tiers 2–3 (Hokusai and Monet), with strict-clean held-out training images per artist (disjoint from the CSD eval anchors), 3000 steps at rank 32, and a per-image caption template "`<movement>` `<medium>`, `<trigger>`, `<audit`

caption>" that does not fix the medium across drawings, prints and paintings within an artist’s oeuvre. At inference we use, as prompts, the rendered captions of the strict-clean anchor set itself, so the prompt distribution matches the distribution against which the generations are evaluated. Pair bidirectional CSD discrimination (generation closer to own than to partner anchor) is the negative-gap metric; top-1 in the 91-class corpus is the positive-control metric.

Negative-gap pair (gap), neg. member	bidir bare-cos	bidir LoRA-cos	bidir LoRA-CSLS
Edo (−0.049), Kawanabe Kyōsai	0/66 ( 0%)	7/60 (12%)	<b>47/60 (78%)</b>
Victorian (−0.039), Frederic Leighton	1/66 ( 2%)	0/57 ( 0%)	3/57 ( 5%)
Russian (−0.030), Isaac Levitan	0/66 ( 0%)	5/60 ( 8%)	6/60 (10%)

Table 6: LoRA stress test, negative-gap pair members against the partner’s strict-clean anchors. The positive-gap members (Sharaku, Godward, Shishkin) reach 100% bidir in every cell and are not shown. Full per-pair / per-condition / per-artist table is in App. D, Tab. 19.

The three negative-gap pairs all reproduce the same asymmetry under raw cosine: the positive-gap pair member reaches 100% pair-bidir discrimination on every generation (Sharaku 69/69, Godward 75/75, Shishkin 63/63 correct on cosine), while the negative-gap member is misclassified against the partner’s anchors in  $\geq 88\%$  of generations (Kyōsai 12% bidir, Leighton 0%, Levitan 8%). LoRA training pushes generations into the CSD region its training material already inhabits; the diagnostic has flagged that region as overlapping with the partner’s, so no amount of training and no choice of `lora_scale` restores the missing separability under raw cosine.

The CSLS readout (§5) partly closes the gap on one of the three negative-gap pairs. On Sharaku/Kyōsai, CSLS lifts Kyōsai pair-bidir from 12% (raw cosine) to 78%, and the readout that §5 validates on *authentic* anchors carries its discrimination benefit over to LoRA generations. On Leighton/Godward and Levitan/Shishkin, CSLS leaves the negative member near zero (5%, 10%): Leighton/Godward in the §7 residual, Levitan/Shishkin recovered diagnostically (anchor gap  $-0.030 \rightarrow +0.003$ ) but not on T2I generations. The pattern provides initial evidence that the §4 gap value is a useful indicator of T2I-readiness: at gap  $-0.049$  (Edo) the structural overlap is partly readout-bound and CSLS recovers it; at  $-0.039$  and  $-0.030$  the overlap is structural and survives every zero-training intervention.

The positive controls confirm the converse only weakly under our inference protocol: bare-Flux Hokusai and Monet sit at 0% top-1 in the 91-class corpus, and the trained LoRAs reach 8% and 15% respectively. This is a measurable trigger lift relative to bare, but short of the Tier-1 regime (Sharaku LoRA 100%, Godward LoRA 96%, Shishkin LoRA 63%) that the bare positive members of the negative-gap pairs reach. The practical implication is that for Tier-2/3 artists LoRA-conditioning provides a real but bounded lift, useful for style imitation, less than the bare-Flux trigger already does for canonical Tier-1 artists.

Two failure modes interact: bare prompting under-conditions T2I except for canonical-and-distinctive artists, and LoRA cannot manufacture, under raw cosine, a CSD distinction the diagnostic has flagged as negative-gap; CSD+ recovers it for readout-correctible pairs, not for residual ones. Practical recipe: before reporting CSD-cosine as a T2I-style-fidelity score on artist  $X$ , run the diagnostic of §4 on the candidate corpus. If  $g_X > 0$ , raw cosine is in a meaningful regime. If  $g_X \leq 0$  but the artist is among the pairs CSD+ rescues, CSLS on pos-interp 336 is the operational readout. If  $g_X \leq 0$  and the pair is in the §7 residual, no zero-training readout will lift CSD-cosine into a calibrated signal; alternative evaluation (human style-comparison on reference exemplars, or movement-level attribution) is required.

## 9 Discussion and Recommendations

The raw cosine of CSD-768 is widely used as an absolute style-fidelity score. The discrimination diagnostic of §4 makes the test for that reading explicit: 23/91 artists in our corpus have a within-class median that sits below the worst cross-class median, and on these artists the absolute reading is order-inverted on at least one within-tradition neighbour. The phenomenon survives the per-image VLM audit, the strict-clean anchor filter, and bootstrap resampling (§§3, 4); it reappears on CLIP-ViT-L/14, SigLIP-large and DINOv2-Large with the same shared-tradition pairs at the worst end (§7). Raw cosine should therefore not be reported as a calibrated absolute style score without first running the corpus-internal diagnostic on the candidate evaluation corpus.

The minimal practical correction is two zero-training readouts on the frozen backbone. CSLS on vanilla 224 is the default: it reduces the aggregated negative-gap count from 15/91 to 4/91 and lifts pair-verification AUC by  $+0.017$  across 25 artist-disjoint splits, at no additional embedding cost. Pos-interp 336 adds a further verification-AUC gain to  $+0.022$  combined (sub-additive). The two levers act on partially overlapping error components: pos-interp recovers truncated spatial evidence, CSLS removes a hubness-style local-density bias. When supervised pairs are available, pair-feature logistic regression on raw 768-d CSD outperforms every cosine-style readout (AUC 0.917, 25/25 splits)

and its dominant feature block is the elementwise  $|a - b|$ . The diagnostic gap also offers initial evidence for T2I-readout evaluability (§8): CSLS recovers the negative-gap pair when the diagnostic places it on the readout-correctible side, not in the residual.

What remains is a small informative residual: three to five artists that survive every zero-training correction, mapping onto known shared-tradition neighbours as cohesive HDBSCAN clusters (§7; App. C). The pattern reproduces across all four backbones, which separate artist or caption labels but lack a within-tradition signal. Counts depend on the artist set; the pattern recurs on any intra-tradition corpus. Run the diagnostic first.

## References

- [1] Black Forest Labs. FLUX.1 image generation models. <https://github.com/black-forest-labs/flux>, 2024. FLUX.1-dev: 12B-parameter rectified-flow transformer; reference code Apache-2.0, model weights under the FLUX.1 [dev] Non-Commercial License.
- [2] Alexis Conneau, Douwe Kiela, Holger Schwenk, Loïc Barrault, and Antoine Bordes. Supervised learning of universal sentence representations from natural language inference data. In *EMNLP*, 2017.
- [3] Alexis Conneau, Guillaume Lample, Marc’Aurelio Ranzato, Ludovic Denoyer, and Hervé Jégou. Word translation without parallel data. In *ICLR*, 2018.
- [4] Elena Facco, Maria d’Errico, Alex Rodriguez, and Alessandro Laio. Estimating the intrinsic dimension of datasets by a minimal neighborhood information. *Scientific Reports*, 7:12140, 2017.
- [5] Leon A. Gatys, Alexander S. Ecker, and Matthias Bethge. Image style transfer using convolutional neural networks. In *CVPR*, 2016.
- [6] Chang Liu, Viraj Shah, Aiyu Cui, and Svetlana Lazebnik. UnZipLoRA: Separating content and style from a single image. In *International Conference on Computer Vision (ICCV)*, 2025. Highlight; arXiv:2412.04465.
- [7] Jiaqi Mu and Pramod Viswanath. All-but-the-top: Simple and effective postprocessing for word representations. In *ICLR*, 2018.
- [8] Maxime Oquab, Timothée Darcet, Théo Moutakanni, Huy Vo, Marc Szafraniec, Vasil Khalidov, Pierre Fernandez, Daniel Haziza, Francisco Massa, Alaaeldin El-Nouby, Mahmoud Assran, Nicolas Ballas, Wojciech Galuba, Russell Howes, Po-Yao Huang, Shang-Wen Li, Ishan Misra, Michael Rabbat, Vasu Sharma, Gabriel Synnaeve, Hu Xu, Hervé Jégou, Julien Mairal, Patrick Labatut, Armand Joulin, and Piotr Bojanowski. DINOv2: Learning robust visual features without supervision. *Transactions on Machine Learning Research*, 2024. arXiv:2304.07193.
- [9] Alec Radford, Jong Wook Kim, Chris Hallacy, Aditya Ramesh, Gabriel Goh, Sandhini Agarwal, Girish Sastry, Amanda Askell, Pamela Mishkin, Jack Clark, Gretchen Krueger, and Ilya Sutskever. Learning transferable visual models from natural language supervision. In *Proceedings of the 38th International Conference on Machine Learning (ICML)*, 2021.
- [10] Miloš Radovanović, Alexandros Nanopoulos, and Mirjana Ivanović. Hubs in space: Popular nearest neighbors in high-dimensional data. *Journal of Machine Learning Research*, 11:2487–2531, 2010.
- [11] Litu Rout, Yujia Chen, Nataniel Ruiz, Abhishek Kumar, Constantine Caramanis, Sanjay Shakkottai, and Wen-Sheng Chu. RB-Modulation: Training-free stylization using reference-based modulation. In *International Conference on Learning Representations (ICLR)*, 2025. <https://openreview.net/forum?id=bnINPG5A32>.
- [12] Nataniel Ruiz, Yuanzhen Li, Neal Wadhwa, Yael Pritch, Michael Rubinstein, David E. Jacobs, and Shlomi Fruchter. Magic insert: Style-aware drag-and-drop. arXiv:2407.02489, 2024.
- [13] Florian Schroff, Dmitry Kalenichenko, and James Philbin. FaceNet: A unified embedding for face recognition and clustering. In *CVPR*, 2015.
- [14] Gowthami Somepalli, Anubhav Gupta, Kamal Gupta, Shramay Palta, Micah Goldblum, Jonas Geiping, Abhinav Shrivastava, and Tom Goldstein. Measuring style similarity in diffusion models. arXiv:2404.01292, 2024.
- [15] Łukasz Staniszewski, Katarzyna Zaleska, and Kamil Deja. Low-rank continual personalization of diffusion models. arXiv:2410.04891, 2024. SCOPE Workshop @ ICLR 2025.
- [16] Haofan Wang, Peng Xing, Renyuan Huang, Hao Ai, Qixun Wang, and Xu Bai. InstantStyle-Plus: Style transfer with content-preserving in text-to-image generation. arXiv:2407.00788, 2024.
- [17] Xiaohua Zhai, Basil Mustafa, Alexander Kolesnikov, and Lucas Beyer. Sigmoid loss for language image pre-training. In *International Conference on Computer Vision (ICCV)*, 2023.

## A Corpus details

The 400-artist list released with the CSD code repository (file `artists_400.txt`) contains 400 raw entries with substantial duplication: the same artist appears repeatedly under different name spellings, e.g. “Mucha”, “Alphonse Mucha” and “Alfonse Mucha”. After canonical-name deduplication 367 distinct artists remain. We augment the list with fourteen non-Western artists from Edo-period Japan (Hokusai, Hiroshige, Utamaro, Sharaku, Itō Jakuchū, Hasegawa Tōhaku, Kawanabe Kyōsai), Ming-dynasty China (Shen Zhou) and modern Chinese ink (Wu Changshuo), Joseon-dynasty Korea (Kim Hong-do), Persian miniature (Behzād), Indian Academic realism (Raja Ravi Varma), and Mexican popular print and Surrealism (Posada, Kahlo). To fill specific under-represented traditions, we further augment with Spanish Baroque (Velázquez, Murillo, Zurbarán), French Romanticism (Delacroix, Géricault), American Tonalism (Whistler, Inness), Cubism (Juan Gris, Robert Delaunay, Albert Gleizes, Jean Metzinger), Mughal miniature (Ustad Mansur), Naive art (Henri Rousseau), Early-Renaissance Italian painting (Botticelli, Mantegna), and additional Symbolist and French Academic entries (Odilon Redon, Gustave Moreau, William-Adolphe Bouguereau). The augmented list is the input to the fetcher.

For each canonical name we attempt a public-domain artwork fetch from Wikimedia Commons via the Wikidata-resolved Commons category, trying structured sub-categories (*Paintings by X*, *Sculptures by X*, *Woodblock prints by X*, etc.) and falling back to the Wikidata-canonical category for the specific artist (never to the bare canonical name, which on Commons often resolves to a disambiguation node such as “Vermeer (surname)” that pulls in homonyms). We fix a target of twenty-five artworks per artist with a hard minimum of fifteen. All retained anchor images and the authentic-work exemplars reproduced in this paper’s figures were obtained from Wikimedia Commons entries carrying public-domain or PD-Art licensing metadata; per-image licence metadata is retained alongside the embedding NPZ.

The fetched candidates are subjected to a two-stage attribution audit. Stage 1 applies regular-expression filters on the filename together with the Wikimedia “Artist” metadata field; Stage 2 sends every borderline file’s textual metadata (image description, object name, categories, permission and credit fields) to a Sonnet-class language-model judge that classifies the entry into one of seven attribution labels: *master*, *workshop*, *school*, *after*, *attributed*, *imitator*, or *off\_topic/wrong\_person*. Of the 2736 candidates across 113 fetched artists, 2273 pass the audit (2107 master, 15 workshop, 7 school, 125 after, 19 attributed). The remaining 463 files are imitator-class works, modern photographs of unrelated subjects, or files that share an artist’s name but depict a different person (a horse named “Wilm Vermeer” is the most striking example).

A second per-image content audit runs on every retained candidate via a local vision–language model (Qwen3-VL-32B-Instruct) with a structured JSON-schema prompt. Each image is classified along four axes: *is\_artwork\_by\_artist* (false flags historical photographs of the artist or their travels, museum-reproduction pages, book covers, memorial plaques and similar non-work imagery), *artwork\_kind*  $\in$  {painting, drawing, watercolor, print, mixed\_media, sculpture, other, photograph}, *has\_frame*, and *has\_museum\_context*. Items flagged as photographs or as not the artist’s own work are dropped; items with the audit-flagged frame or museum-context channels are also dropped from the anchor set so that frame pixels do not leak into the embedding under multi-crop or pos-interp readouts. On the post-attribution pool the content audit removes about 20% of the images overall (concentrated in artists whose Commons pages are dominated by archive photographs of the painter, framed museum-display shots and book-cover scans rather than autograph artworks), leaving 1799 admissible strict-clean anchors. Artists whose post-audit pool falls below ten anchors are dropped from the working corpus; together with the fifteen-anchor minimum at the attribution stage this pipestep removes twenty-two artists in total (including Otto Dix, Marcel Duchamp, Jean Arp, Caravaggio, Frida Kahlo, Leonardo da Vinci, Sesshū Tōyō, Qi Baishi; and, post-strict-cleaning, William Morris (decorative-design oeuvre dominated by “other” artwork-kind classifications), Rembrandt (8 strict-clean anchors after frame/museum removal) and Gustave Moreau (9)). The remaining fetched-but-rejected artists divide into entries with no Wikimedia presence at all (predominantly contemporary digital illustrators whose works are under copyright) and the audit-and-minimum dropouts described above. Fig. 4 summarises the cascade.

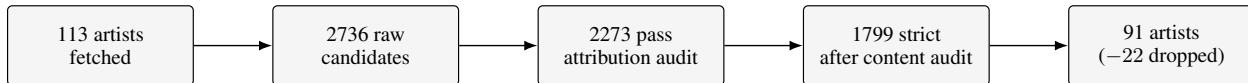


Figure 4: Corpus pipeline. Stages: Wikimedia fetch; attribution audit (regular-expression filter and language-model attribution judge); content audit (per-image vision–language model); ten-anchor strict-clean floor. The 22 dropped artists (including William Morris, Rembrandt, Gustave Moreau post-strict-cleaning, and twelve already removed at the attribution stage) are listed in the prose above.

For each of the 91 retained artists we manually attach a primary art-movement or tradition label drawn from a 47-label vocabulary covering the major Western traditions (Hudson River School, Pre-Raphaelite, Vienna Secession,

Dadaism, etc.) and the non-Western categories the corpus addition introduces (Edo-period Japan, Momoyama-period Japan, Muromachi-period Japan, Meiji-period Japan, Ming-dynasty China, Late-Qing China, modern Chinese ink, Joseon-dynasty Korea, Persian miniature, Indian Academic Realism, Mexican popular print). Movement labels are author-curated from standard art-historical references; borderline cases such as Modigliani as “Modernism” rather than “School of Paris” or Hubert Robert as “Romanticism” rather than “Pre-Romantic” are defensible but not unique. Each artist enters the aggregate statistics only once, so the headline numbers are robust to single-artist re-classification; absolute purity values for individual clusters in App. C would shift by at most a few percentage points under reasonable label revisions and would not change the qualitative ranking among methods.

**The 91 retained artists, by primary movement.** *18th-century Italian:* Piranesi. *American Realism:* Hopper, Tanner, Eakins, Homer. *American Tonalism:* Inness, Whistler. *Art Nouveau:* Mucha, Tiffany. *Baroque:* La Tour, Rubens. *Biedermeier:* Spitzweg. *Cubism:* Gleizes, Gris, Delaunay. *Dadaism:* Picabia. *Dutch Golden Age:* Hals, Vermeer. *Early Renaissance:* Mantegna, Fra Angelico, Botticelli. *Edo-period Japan:* Hokusai, Jakuchū, Utamaro, Sharaku, Hiroshige. *French Academic:* Aublet, Bouguereau. *French Romanticism:* Delacroix, Géricault. *German Realism:* Baluschek. *Golden Age Illustration:* Dulac, Parrish. *High Renaissance:* Raffaello, Titian. *Hudson River School:* Bierstadt, Church, Heade, Gifford, Cole. *Impressionism:* Monet, Sargent, Cassatt. *Indian Academic Realism:* Varma. *Joseon-dynasty Korea:* Kim Hong-do. *Mannerism:* Arcimboldo. *Meiji-period Japan:* Kyōsai. *Mexican Muralism:* Rivera. *Mexican popular print:* Posada. *Ming-dynasty China:* Shen Zhou. *Modernism:* Modigliani. *Momoyama-period Japan:* Tōhaku. *Mughal miniature:* Mansur. *Naive Art:* Rousseau. *Northern Renaissance:* Bosch, van Eyck. *Persian miniature:* Behzād. *Post-Impressionism:* Seurat, Van Gogh. *Pre-Raphaelite:* Rossetti, De Morgan, Waterhouse. *Realism:* Courbet. *Romanticism:* Friedrich, Knab, Goya, Doré, H. Robert, Lawrence, Blake, Turner. *Russian Realism:* Kuindzhi, Repin, Levitan, Shishkin. *Russian Romanticism:* Aivazovsky. *Russian Symbolism:* Bilibin, Vrubel, Vasnetsov. *Spanish Baroque:* Murillo, Velázquez, Zurbarán. *Surrealism:* Tanguy. *Symbolism:* Bussiere, Redon. *Victorian Academic:* Leighton, Godward. *Victorian Fairy Painting:* Fitzgerald. *Victorian Realism:* Grimshaw. *Vienna Secession:* Klimt. *Western American:* C. M. Russell.

Wikimedia Commons coverage is uneven across the 91 retained artists: Rubens, Goya and Klimt each have several hundred public-domain works indexed on Commons, while less canonical artists in the same public-domain era are represented by fewer than thirty. After all attribution and content audits are applied (the two-stage attribution audit above plus the per-image content audit), the working pool holds the post-audit strict-clean set per artist, capped at 30 admissible images: artists whose audited pool exceeds 30 are downsampled quality-first (frame-/museum-context-free preferred), and artists whose post-audit pool falls short are kept as-is provided they clear the ten-anchor strict-clean floor. The resulting per-artist counts have median = 20 and lie in [11, 27]. We do not weight the downstream analysis by sample reliability: an artist with thirty broadly-sampled works available is described by a more representative sample of their oeuvre than one with thirty narrowly-themed works.

**Per-artist bootstrap CIs for the discrimination gap.** §4 reports the aggregate negative-gap count under bootstrap resampling ( $21.9 \pm 2.7$  across 100 resamples). Tab. 7 extends this to per-artist 95%-confidence intervals on  $g_k$ , drawn from the same resampling scheme (seed 0). Of the 23 artists with a negative point-estimate, 2 have CIs that lie entirely below zero (robust\_negative: Delacroix, Kyōsai); the remaining 21 have CIs that cross zero, so although their point-estimate is negative, the within-class anchor count ( $n_k \in [11, 25]$  for the bottom of the distribution) does not certify negativity at 95% confidence. The shared-tradition pattern that §4 characterises is therefore visible at the population level (count of negative gaps is reproducible across resamples) but not always certifiable at the individual-artist level for points near the decision boundary.

**Sensitivity to the artist-pool composition.** Because  $c_k$  is a maximum over other artists, a candidate corpus that includes a stylistically close artist can lower  $g_k$ , while a corpus that omits one can raise it. We therefore probe the discrimination gap’s sensitivity to the artist set itself. Tab. 8 reports three checks. Under leave-one-artist-out (S1), removing any single artist from the pool shifts the aggregate neg-gap fraction by less than one percentage point on average; only 2 of the 15 main-text Tab. 1 artists flip to a positive gap when their worst-other is removed (Delacroix when Goya is removed, Itō Jakuchū when Sharaku is removed), and the remaining 13 stay negative. Under random 70-artist subsamples (S2, 100 resamples, seed 0) the neg-gap fraction is  $0.23 \pm 0.027$ , range [10, 21] artists, on the same order as the bootstrap-resampling estimate of §4. Under the same subsamples (S3), the worst-other identity for each of the 23 negative-gap artists is preserved in 100% of runs where both artists are in the sub-pool, and the gap remains negative in 100% of those runs. The shared-tradition pairs that the diagnostic flags are therefore geometrically intrinsic rather than artefacts of the specific artist set we tested.

**CSLS pool sensitivity.** Because CSLS is reference-pool-dependent, we repeat the subsample analysis for the CSLS-aggregated gap. The four CSLS-neg-gap artists on the full 91-pool are Botticelli, Leighton, Velázquez and Kyōsai

Levitan, *Golden Autumn. Slobodka* (1889)Shishkin, *Morning in a Pine Forest* (1889)Levitan, *Birch Grove* (1885–1889)Shishkin, *A Pine Forest, Mast-Timber Forest* (1872)

Figure 5: Why CSD confuses Isaac Levitan with Ivan Shishkin (gap  $-0.030$  in main-text Tab. 1). Both are nineteenth-century Russian Realist landscape painters; the shared subject vocabulary (birch and pine forests, atmospheric light, ground-level vantage) and the shared compositional logic (deep recession, low horizon, dense foliage) are the gradient signal that CSD’s contrastive training amplifies. The distinguishing features (Levitan’s softer chromatic register and looser handling against Shishkin’s botanical precision) are the residual that artist-level discrimination needs to recover, and that the embedding’s median cosine does not. All four works are reproduced from Wikimedia Commons entries carrying public-domain or PD-Art licensing metadata.

(gaps  $-0.035$  to  $-0.006$ ). Tab. 9 reports the same three setups. Under leave-one-artist-out the CSLS-neg-gap fraction is  $0.044 \pm 0.003$ , essentially invariant. Under random 70-artist subsamples it is  $0.03 \pm 0.014$  (count range  $[0, 4]$ ). The worst-other identity is preserved in 100% of subsamples for all four artists, and the gap remains negative in 97% of conditional runs (100% for Botticelli and Leighton, 92% for Velázquez, 94% for K y sai). CSLS is therefore at least as pool-robust as raw cosine; the residual after CSD+ is not an artefact of the candidate-pool composition.

## B Full CSD+ readout grid and ablations

**Full  $6 \times 4$  readout grid.** The compact  $4 \times 3$  form in the main text (Tab. 3) shows the negative-gap count for the three operational input pipelines (vanilla 224, multi-crop  $5 \times 224$ , pos-interp 336) crossed with the four score-level variants. Tab. 10 below adds the two intermediate pos-interp resolutions (280, 392) and the high resolution (448) that the scale ablation explores, plus the per-cell median gap.

**Scale ablation.** Bilinear interpolation of the trained positional embeddings to a  $g \times g$  grid permits inference at  $14g \times 14g$  on the same backbone weights. Tab. 11 reports the diagnostic and verification AUC at five grid sizes. The discrimination diagnostic improves monotonically up to  $\approx 280$  and saturates by 336; verification AUC peaks at 280–336 and *degrades* beyond 336. The two best CSLS-AUC cells are practically tied within sampling noise:  $0.907 \pm 0.016$  at 280 and  $0.905 \pm 0.016$  at 336, indistinguishable on the same 25 splits. We adopt 336 as the operational recipe because it sits at the saturating shoulder of the curve and is the more robust of the two against split-by-split variance. We do not recommend going beyond 336.

**Multi-crop aggregation versus pos-interp.** Replacing the single centre crop with five  $224 \times 224$  crops sampled from a  $256 \times 256$  base (the four corners plus the centre), embedding each crop independently and averaging the embeddings, recovers some of the spatial coverage that the single centre crop loses. Read as a Monte-Carlo estimator of

Artist	$n$	$w_k$	$c_k$	Worst other	Gap $g_k$	95% CI	Cls
Mikhail Vrubel	14	+0.149	+0.247	Louis Comfort Tiffany	-0.098	[-0.167, +0.083]	○
Raffaello Sanzio	18	+0.335	+0.420	Andrea Mantegna	-0.085	[-0.120, +0.087]	○
Eugène Delacroix	23	+0.372	+0.455	Francisco Goya	-0.083	[-0.115, -0.013]	●
Hasegawa Tōhaku	12	+0.420	+0.494	Tōshūsai Sharaku	-0.074	[-0.122, +0.012]	○
Sandro Botticelli	15	+0.318	+0.389	Andrea Mantegna	-0.071	[-0.146, +0.068]	○
Ivan Bilibin	23	+0.258	+0.313	José Guadalupe Posada	-0.055	[-0.098, +0.010]	○
Kawanabe Kyōsai	20	+0.479	+0.527	Tōshūsai Sharaku	-0.049	[-0.078, -0.000]	●
Gustave Doré	23	+0.277	+0.317	Francisco Goya	-0.040	[-0.140, +0.006]	○
Frederic Leighton	19	+0.253	+0.293	John William Waterhouse	-0.040	[-0.093, +0.033]	○
Maxfield Parrish	25	+0.339	+0.379	Kitagawa Utamaro	-0.039	[-0.158, +0.109]	○
Isaac Levitan	20	+0.289	+0.319	Ivan Shishkin	-0.030	[-0.061, +0.027]	○
Albert Aublet	18	+0.228	+0.257	Francisco Goya	-0.029	[-0.080, +0.070]	○
Diego Velázquez	17	+0.385	+0.409	Georges de La Tour	-0.024	[-0.075, +0.050]	○
Itō Jakuchū	11	+0.463	+0.482	Tōshūsai Sharaku	-0.019	[-0.061, +0.075]	○
Gustav Klimt	20	+0.283	+0.301	Odilon Redon	-0.019	[-0.090, +0.091]	○
Albert Bierstadt	24	+0.401	+0.417	George Inness	-0.016	[-0.044, +0.035]	○
John Singer Sargent	18	+0.270	+0.284	Edward Hopper	-0.014	[-0.080, +0.028]	○
Utagawa Hiroshige	19	+0.570	+0.578	Kitagawa Utamaro	-0.008	[-0.066, +0.067]	○
Henry Ossawa Tanner	23	+0.260	+0.267	James McNeill Whistler	-0.007	[-0.039, +0.024]	○
Frederic Edwin Church	19	+0.473	+0.480	Thomas Cole	-0.007	[-0.067, +0.040]	○
Jan van Eyck	18	+0.392	+0.395	Andrea Mantegna	-0.003	[-0.028, +0.076]	○
Peter Paul Rubens	17	+0.427	+0.428	Bartolomé Esteban Murillo	-0.001	[-0.053, +0.049]	○
Johannes Vermeer	12	+0.415	+0.416	Georges de La Tour	-0.001	[-0.051, +0.168]	○

Table 7: Full table of all 23 negative-point-estimate-gap artists, sorted ascending by gap ( $g_k = w_k - c_k$ ;  $w_k$  = within-class median pairwise cosine,  $c_k$  = maximum cross-class median cosine). 95% CIs from 100 bootstrap resamples (seed 0). CIs: ● = robust\_negative (CI upper < 0), ○ = ambiguous (CI contains 0). Of 91 artists, 23 have negative point estimate; 2 are robust\_negative under bootstrap.

Setup	Finding
S1: Leave-one-out (91 runs), neg-gap fraction per run	Full pool: 0.25; LOO mean: 0.25 ( $\pm 0.005$ ); 2/15 main-text Tab. 1 artists flip to $g_k > 0$ when worst-other removed
S2: Random 70-artist subsample (100 runs, seed 0)	Neg-gap fraction: $0.23 \pm 0.027$ ; count range [10–21]
S3: Worst-other identity stable across subsamples	Mean stability 100%; gap remains negative in 100% of runs (when both artist and worst-other in pool)

Table 8: Sensitivity of the discrimination gap  $g_k = w_k - c_k$  to artist-pool variation. S1: leaving one artist out at a time shifts the neg-gap fraction negligibly; the worst-other identity drives results (only 2/15 main-text Tab. 1 gaps flip when the worst-other is removed). S2: random 70-artist subsamples yield stable neg-gap fraction. S3: worst-other identity persists in  $\approx 100\%$  of subsamples where both artists appear.

the crop-distribution mean  $z = \mathbb{E}_c[\phi(x_c)]$ , the  $K$ -crop average has variance  $\text{Var}(\hat{z}) = \frac{\sigma^2}{K} [1 + (K-1)\bar{\rho}]$ , where  $\sigma^2$  is the per-crop variance under crop position and  $\bar{\rho}$  is the average between-crop correlation. The five-crop construction draws all crops from a  $256 \times 256$  base, so the crops overlap substantially and  $\bar{\rho}$  is large; the bracketed factor stays well above the 1-of- $K$  ideal achievable with independent crops, and the variance reduction is real but heavily attenuated. More importantly, multi-crop is a *variance* reduction at fixed *bias*: every crop still discards image content outside the  $256 \times 256$  base, so any structural error from truncating peripheral pixels is shared across all  $K$  samples and survives the average. Pos-interp 336, by contrast, removes the truncation bias outright by enlarging the input field rather than sampling within a fixed one. Where the dominant readout error is truncation bias rather than crop-position variance, multi-crop optimises the wrong axis of the error decomposition.

**Full verification-robustness statistics.** Tab. 12 expands main-text Tab. 4 with the AUC range, EER and full paired-comparison statistics that the prose of §6 relies on but that the slim inline table omits.

Setup	Finding
S1: Leave-one-out (91 runs, CSLS $k = 15$ ), neg-gap fraction per run	Full pool: 0.04; LOO mean: 0.04 ( $\pm 0.003$ ); all 4 CSLS-neg-gap artists flip to $g_k > 0$ when their worst-other removed
S2: Random 70-artist subsample (100 runs, seed 0)	Neg-gap fraction: $0.03 \pm 0.014$ ; count range [0–4]
S3: Worst-other identity stable across subsamples	Mean stability 100%; gap remains negative in 97% of runs (when both artist and worst-other in pool)

Table 9: Sensitivity of the CSLS-aggregated gap ( $k = 15$ ) to artist-pool variation (vanilla 224 embedding, 91 artists). S1: leaving one artist out shifts the CSLS-neg-gap fraction by  $\pm 0.003$ ; all 4 CSLS-neg-gap artists flip positive when their single worst-other confuser is removed. S2: random 70-artist subsamples yield a stable neg-gap fraction. S3: worst-other identity persists in  $\approx 100\%$  of subsamples, confirming pool-robustness of the CSLS readout.

Embedding	Score variant	# neg	median gap
vanilla 224	cosine	15	+0.075
vanilla 224	CSLS	4	+0.187
vanilla 224	cohort- $z$	15	+0.516
vanilla 224	margin	5	+0.127
5-crop avg 224	cosine	11	+0.078
5-crop avg 224	CSLS	5	+0.201
5-crop avg 224	cohort- $z$	11	+0.488
5-crop avg 224	margin	4	+0.136
pos-interp 280	cosine	10	+0.082
pos-interp 280	CSLS	4	+0.198
pos-interp 280	cohort- $z$	10	+0.489
pos-interp 280	margin	3	+0.140
pos-interp 336	cosine	11	+0.082
pos-interp 336	CSLS	5	+0.195
pos-interp 336	cohort- $z$	11	+0.558
pos-interp 336	margin	5	+0.136
pos-interp 392	cosine	11	+0.081
pos-interp 392	CSLS	3	+0.186
pos-interp 392	cohort- $z$	11	+0.541
pos-interp 392	margin	3	+0.135
pos-interp 448	cosine	14	+0.076
pos-interp 448	CSLS	3	+0.185
pos-interp 448	cohort- $z$	14	+0.496
pos-interp 448	margin	4	+0.123

Table 10: Full CSD+ grid: every input-pipeline variant crossed with every score-level variant on the discrimination diagnostic. # neg is the count, out of 91 artists, with negative aggregated discrimination gap; median gap is the median over artists. The diagnostic is deterministic on the full 91-artist corpus and does not depend on a held-out split. The compact form summarised in the main text (Tab. 3) drops the median-gap column and keeps only the three input pipelines (*vanilla 224*, *multi-crop 5 × 224*, *pos-interp 336*); pos-interp 280 / 392 / 448 add only marginal variation in CSLS and the operational recipe collapses to the same point. Verification AUCs for the cosine and CSLS variants are reported in main-text Tab. 4 (and Tab. 12 below with full per-split statistics) as mean  $\pm$  std across 25 artist-disjoint splits.

**Hard-negative regimes.** Tab. 13 expands the hard-negative discussion of §6 with the full four regimes (random, same-movement, worst-neighbour, positive-gap control) crossed with the three readouts (cosine vanilla 224, CSLS on pos-interp 336, pair-feature logistic regression on pos-interp 336). The worst-neighbour regime is the within-tradition stress test that §4 predicts to be hard; it drops AUC by about 0.18 absolute on cosine vanilla and CSLS narrows the gap by the same fraction as in the random regime. Same-movement is essentially indistinguishable from random under the strict-clean corpus; the positive-gap control verifies that artists with a clean diagnostic ( $g_k > 0.05$ ) reach AUC above 0.92 across all readouts.

input size	# neg gap (cos)	cos AUC	# neg gap (CSLS)	CSLS AUC
224 (vanilla)	15	0.883 ± 0.016	4	0.900 ± 0.016
280	10	0.895 ± 0.016	4	<b>0.907 ± 0.016</b>
336 (recipe)	11	0.895 ± 0.016	5	0.905 ± 0.016
392	11	0.890 ± 0.018	3	0.901 ± 0.017
448	14	0.883 ± 0.019	3	0.894 ± 0.019

Table 11: Scale ablation for the pos-interp input variant. Cosine and CSLS verification AUC are reported as mean ± std over the same 25 artist-disjoint splits used for main-text Tab. 4; the vanilla 224 row matches that table by construction. The improvement saturates between 280 and 336 and reverses beyond it, consistent with positional-embedding extrapolation degrading when the grid moves too far from its trained  $16 \times 16$  size. AUCs are computed on the strict-anchor 91-artist corpus, so they exceed the comparable values reported on noisier earlier sweeps.

Method	AUC mean ± std	AUC range	EER mean ± std
Cosine on vanilla CSD (224)	0.883 ± 0.016	[0.848, 0.912]	0.197 ± 0.017
CSLS on vanilla CSD (224)	0.900 ± 0.016	[0.870, 0.930]	0.182 ± 0.018
Cosine on pos-interp 336 (CSD+)	0.895 ± 0.016	[0.858, 0.929]	0.183 ± 0.016
CSLS on pos-interp 336 (CSD+)	0.905 ± 0.016	[0.874, 0.939]	0.175 ± 0.017
Pair-logreg on vanilla CSD (224)	0.917 ± 0.018	[0.878, 0.952]	0.163 ± 0.021
Pair-logreg on pos-interp 336	0.917 ± 0.017	[0.874, 0.951]	0.165 ± 0.019

Left method	Right method	wins/25	mean $\Delta$	95% CI
Pair-logreg vanilla	Cosine vanilla	25	+0.0343	[+0.0308, +0.0377]
CSLS vanilla	Cosine vanilla	25	+0.0168	[+0.0141, +0.0196]
Cosine pos-interp 336	Cosine vanilla	24	+0.0118	[+0.0099, +0.0137]
CSLS pos-interp 336	Cosine vanilla	25	+0.0221	[+0.0190, +0.0252]
Pair-logreg pos-interp 336	Cosine vanilla	25	+0.0339	[+0.0302, +0.0377]
Pair-logreg pos-interp 336	Pair-logreg vanilla	11	-0.0004	[-0.0018, +0.0011]
CSLS pos-interp 336	CSLS vanilla	24	+0.0053	[+0.0040, +0.0065]
CSLS pos-interp 336	Pair-logreg vanilla	0	-0.0122	[-0.0136, -0.0107]

Table 12: Per-method statistics for the verification robustness study (§6, 25 artist-disjoint splits on the 91-artist corpus). Top: mean±std AUC, AUC range, and EER. Bottom: paired-split comparisons. 95% CIs are computed as  $\bar{\Delta} \pm t_{24,0.025} \cdot \text{sd}(\Delta) / \sqrt{25}$  and exclude zero for every cell except pair-logreg pos-interp 336 vs pair-logreg vanilla, where  $\bar{\Delta} \approx 0$  confirms input-upgrade indifference.

**Pair-feature ablation across 25 splits.** Pair-feature logistic regression on  $\phi(a, b) = [|a - b|, a \odot b, (a + b)/2]$  reaches AUC  $0.917 \pm 0.018$  on raw 768-d CSD across 25 splits.

**Embedding-postproc baselines.** Standard embedding-postprocessing recipes from the word-embedding literature act on the embedding vectors directly rather than on the readout, and we report them as baselines against the score-level CSD+ family. Centering (subtract corpus mean,  $L^2$ -normalise), all-but-the-top [7] (remove top- $k$  principal directions), and PCA whitening (project to top- $d$  principal directions, divide by  $\sqrt{\text{eigenvalue}}$ ) are all considered. Held-out, fitting on the 73 training artists per split and applying to the 18 test artists in the verification protocol of §6: centering raises cosine verification AUC by approximately +0.02 across the splits, but does *not* reduce the aggregated negative-gap count, which is the primary diagnostic-side improvement CSLS provides (main-text Tab. 3). Centering is therefore a complement to CSD+ on the verification side, not a substitute on the diagnostic side. ABTT-3 *loses* verification AUC (−0.006 on cosine, −0.029 on pair-logreg) and PCA whitening with 128 or 256 components loses 0.02–0.04 on both readouts; transductive variants improve the discrimination diagnostic but do not generalise to held-out artists, exactly the pattern §6 documents for UMAP-projected features.

**CSLS  $k$ -sensitivity.** The CSLS readout has one hyperparameter, the neighbourhood size  $k$  at which local densities are estimated. We use  $k = 15$  throughout the main text. Tab. 14 sweeps  $k \in \{5, 10, 15, 20, 50\}$  on both input variants. On vanilla 224 (the default of §5) the aggregated negative-gap count varies between 4 and 5, the pairwise count between 8 and 11, and the median pairwise CSLS gap stays in [+0.165, +0.175]. On pos-interp 336 the corresponding ranges are 3–5, 7–11, and [+0.165, +0.181]. The readout is therefore not sensitive to the choice of  $k$  on either variant; the main-text headline “15/91  $\rightarrow$  4/91 under CSLS” is the  $k = 15$  row of the vanilla-224 block.

Negative-pair regime	Cosine (224)	CSLS (CSD+)	Pair-logreg (CSD+)
Random different artist	0.882 ± 0.014	0.904 ± 0.016	0.916 ± 0.016
Same-movement different artist	0.882 ± 0.019	0.906 ± 0.021	0.917 ± 0.021
Worst-neighbour ( $B = \arg \max_j c_{k,j}$ )	0.696 ± 0.021	0.738 ± 0.022	0.750 ± 0.029
Positive-gap control ( $g_k > 0.05$ )	0.928 ± 0.015	0.947 ± 0.013	0.953 ± 0.013

Table 13: Verification AUC under four negative-sampling regimes on the same 25 artist-disjoint test splits as main-text Tab. 4, on the 91-artist corpus, with regime-specific negative-pair sampling (so the random-regime cosine row  $0.882 \pm 0.014$  matches main-text Tab. 4’s  $0.883 \pm 0.016$  within sampling noise). Same-movement remains high-variance because few test artists cover enough movements per split.

Variant	$k$	agg. neg-gap (of 91)	pairwise neg-gap (of 91)	median pairwise gap
<i>vanilla 224 (default in main text)</i>				
	5	5	8	+0.168
	10	4	9	+0.170
	<b>15</b>	<b>4</b>	<b>8</b>	<b>+0.171</b>
	20	5	8	+0.175
	50	5	11	+0.165
<i>pos-interp 336 (stronger optional recipe)</i>				
	5	3	8	+0.165
	10	5	7	+0.181
	<b>15</b>	<b>5</b>	<b>10</b>	<b>+0.179</b>
	20	4	10	+0.180
	50	4	11	+0.170

Table 14: CSLS  $k$ -sensitivity on both input variants. Default  $k = 15$  row in bold; counts and medians are over the 91 artists.

## C Manifold geometry, clustering and cluster compositions

**Intrinsic dimensionality.** The two-nearest-neighbour estimator of Facco et al. [4] computes, for each sampled point  $x_i$ , distances  $r_1(x_i)$  and  $r_2(x_i)$  to its first and second nearest neighbours, defines  $\mu_i = r_2(x_i)/r_1(x_i)$ , and exploits the fact that on a locally-Euclidean  $d$ -dimensional manifold the distribution of  $\mu_i$  follows a Pareto law of the form  $P(\mu) = d\mu^{-(d+1)}$  for  $\mu \geq 1$ . Cumulating gives  $\Pr(\mu_i \leq \mu) = 1 - \mu^{-d}$ , so  $d$  can be estimated as the slope of  $-\log(1 - F(\mu))$  against  $\log \mu$ , where  $F$  is the empirical CDF over the sample. Applied to twenty independent random subsamples of 1500 of our 1799 points each, the estimator returns ID =  $1.62 \pm 0.91$ , with a per-subsample range of  $[0.72, 2.98]$ . The two-NN estimator is known to be sensitive to small-sample bias on finite samples drawn from low-dimensional manifolds, and we do not read the small absolute values ontologically. What is robust across every subsample is the qualitative claim that the data sits on a low-dimensional manifold inside the 768-d ambient space. The principal-component spectrum is consistent: the top three components explain only 7.2%, 5.4% and 4.9% of variance respectively, totalling 17.6%, so the variance is spread thinly across many linear directions rather than concentrated along a few that matter for style, the qualitative signature of a curved manifold.

**Full clustering sweep.** Tab. 15 reports adjusted Rand index and normalised mutual information against artist labels and against art-movement labels for ten clustering pipelines. We report ARI and NMI rather than purity because they correct for chance agreement at the relevant number of clusters, which varies across methods. The methods cover three approaches to the same underlying question: cluster artists in CSD’s output space.

**ARI computation note.** HDBSCAN-style methods produce a  $-1$  “noise” label for points that do not belong to any high-density region. We compute ARI on the *full* corpus, treating the  $-1$  label as a single class of its own. This is the fair cross-method comparison: a method that labels half the corpus as noise pays for that decision in the ARI formula because the noise points form one giant cluster against which the artist labels score poorly. An earlier version of this analysis reported ARI on the non-noise subset only, which inflated high-noise methods, in particular NMF, which labels 73.9% of the corpus as noise; we correct that here.

The pattern in the table is more nuanced than “linear methods fail, non-linear methods work”. The strongest global pipeline is graph-based on a non-linear projection (Spectral-20D + Leiden,  $r = 1.5$ , ARI 0.209 at the canonical seed of Tab. 15); density clustering on a linear projection fails completely (RandProj-100 + HDBSCAN at ARI 0.003, NMF + HDBSCAN at 0.010); but *hierarchical* clustering on a linear projection is competitive (RandProj-100 + average-linkage

Method	#cl	%noise	ARI(art)	NMI(art)	ARI(mov)	NMI(mov)
Spectral-20D + Leiden, $r=1.5$	30	0.0%	+0.209	+0.615	+0.030	+0.141
Spectral-20D + Leiden, $r=1.0$	28	0.0%	+0.194	+0.609	+0.030	+0.133
RandProj-100 + avg-link, $K=120$	120	0.0%	+0.182	+0.640	+0.028	+0.184
UMAP-20D + HDBSCAN	51	13.5%	+0.150	+0.652	+0.025	+0.209
Correlation-kNN + Leiden, $r=1.5$	17	0.0%	+0.144	+0.556	+0.031	+0.096
Spectral-20D + Leiden, $r=0.5$	18	0.0%	+0.141	+0.562	+0.028	+0.100
UMAP-50D + HDBSCAN	49	13.8%	+0.141	+0.635	+0.025	+0.200
Cosine-kNN + Leiden, $r=1.5$	19	0.0%	+0.138	+0.567	+0.025	+0.098
RandProj-100 + avg-link, $K=80$	80	0.0%	+0.135	+0.582	+0.024	+0.139
Cosine-kNN + Leiden, $r=1.0$	13	0.0%	+0.106	+0.524	+0.023	+0.076
Correlation-kNN + Leiden, $r=1.0$	14	0.0%	+0.102	+0.519	+0.029	+0.091
RandProj-100 + avg-link, $K=40$	40	0.0%	+0.073	+0.469	+0.013	+0.072
Cosine-kNN + Leiden, $r=0.5$	8	0.0%	+0.070	+0.450	+0.024	+0.059
Correlation-kNN + Leiden, $r=0.5$	7	0.0%	+0.066	+0.434	+0.020	+0.041
Spectral-20D + HDBSCAN	35	31.5%	+0.064	+0.546	+0.017	+0.176
NMF-20D on $ X $ + HDBSCAN	23	64.9%	+0.010	+0.350	+0.003	+0.120
RandProj-100 + HDBSCAN	2	25.3%	+0.003	+0.058	+0.002	+0.010

Table 15: Clustering pipelines compared on the 91-artist corpus. ARI and NMI are computed on the full corpus against artist labels (1799 points, 91 classes) and against art-movement labels (47 movements drawn from the corpus-author vocabulary), treating HDBSCAN’s  $-1$  noise label as a single class so high-noise methods do not get scored on the easy interior alone.  $r$  denotes the Leiden resolution parameter. Spectral-20D + Leiden is consistently strongest by global ARI(art); UMAP-20D + HDBSCAN is the more interpretable pipeline because the noise label flags marginal works explicitly.

at  $K=120$  reaches ARI 0.182, within the same band as UMAP-20D + HDBSCAN at 0.150). The structural distinction is therefore not linear versus non-linear projection alone; it is whether the chosen clusterer can tolerate the geometry it is handed. Random projection from 768 to 100 dimensions delivers exactly what JL guarantees: pairwise distances preserved up to  $(1 \pm \epsilon)$ , which is all that hierarchical clustering needs (it merges greedily by Euclidean distance and never queries local density). HDBSCAN on the same RandProj-100 input fails essentially completely because density estimation requires the *rank order* of distances within each neighbourhood to be preserved (which point is closest, second-closest, third-closest), and JL provides no such guarantee on a curved manifold.

Across ten random seeds, Spectral-20D + Leiden  $res = 1.5$  is the strongest by full-corpus ARI at  $0.196 \pm 0.005$  (the 0.209 in Tab. 15 is the canonical-seed value, within one standard deviation of the ten-seed mean), with deterministic-style spread; UMAP-20D + HDBSCAN follows at  $0.145 \pm 0.015$  with the cluster count averaging 68 and 17% noise rate, and UMAP-50D + HDBSCAN is comparable at  $0.143 \pm 0.011$ . We treat both UMAP-20D + HDBSCAN and Spectral-20D + Leiden as defensible recipes for art-historical discovery: the former is more interpretable cluster-by-cluster because HDBSCAN’s noise label flags marginal works honestly, the latter is stronger on the global ARI metric and assigns every point.

**Cluster compositions.** Tab. 16 reports the 12 largest UMAP-20D + HDBSCAN clusters at the canonical seed (`random_state=42`). “Purity” denotes the fraction of points in a cluster whose movement label matches the cluster’s majority movement.

A striking cluster is number 10, a 66-point grouping with 67% Cubism purity composed of Juan Gris (26), Francis Picabia (20) and Albert Gleizes (17), the early-twentieth-century cohort where pictorial conventions transfer across signatures. The pipeline finds this stylistic family without ever seeing the movement labels. Cluster 49 (Early Renaissance, 36 points, 69% purity) groups Andrea Mantegna (17), Sandro Botticelli (7), Raffaello Sanzio (6), Jan van Eyck (3) and Hieronymus Bosch (2), including the Mantegna/Raffaello pair that the diagnostic flags at gap  $-0.085$ . Cluster 21 (Ming-dynasty China and Edo Japan, 30 points, 57% purity) collapses Shen Zhou (17), Kawanabe Kyōsai (4), Hasegawa Tōhaku (3) and Itō Jakuchū (2) into a single East-Asian brush-painting cluster, the very artists that §4 flags as mutually confused. Cluster 41 (Spanish Baroque / Dutch Golden Age, 59 points, 41% purity) groups Georges de La Tour (18), Johannes Vermeer (10), Diego Velázquez (9), Francisco de Zurbarán (9) and Bartolomé Esteban Murillo (6) into a single tenebrism cluster, recovering the Velázquez/La Tour pair that §4 also flags. Cluster 42 (Pre-Raphaelite, 84 points, 62% purity) groups Dante Gabriel Rossetti (19), William-Adolphe Bouguereau (18), Evelyn De Morgan (17), John William Waterhouse (16) and Frederic Leighton (5), recovering the Leighton/Waterhouse pair the diagnostic flags. The largest cluster, number 23 with 321 points and 20% movement purity, is the Hudson-River-School / American-Tonalism / Russian-Romantic landscape cluster (Spitzweg, Cole, Bierstadt, Aivazovsky and Shishkin),

Cluster	$n$	Purity	Majority movement	Top-5 artists
23	321	0.20	Hudson River School	Carl Spitzweg(23), Thomas Cole(23), Albert Bierstadt(22), Ivan Aivazovsky(19), Ivan Shishkin(19)
42	84	0.62	Pre-Raphaelite	Dante Gabriel Rossetti(19), William-Adolphe Bouguereau(18), Evelyn De Morgan(17), John William Waterhouse(16), Frederic Leighton(5)
10	66	0.67	Cubism	Juan Gris(26), Francis Picabia(20), Albert Gleizes(17), Diego Rivera(2), Robert Delaunay(1)
26	63	0.43	Romanticism	Francisco Goya(25), Eugène Delacroix(12), Piranesi(9), Raffaello Sanzio(3), Frederic Leighton(2)
41	59	0.41	Spanish Baroque	Georges de La Tour(18), Johannes Vermeer(10), Diego Velázquez(9), Francisco de Zurbarán(9), Bartolomé Esteban Murillo(6)
32	48	0.38	Post-Impressionism	Georges Seurat(18), Claude Monet(15), Gustav Klimt(6), Isaac Levitan(3), John Singer Sargent(3)
45	37	0.51	American Realism	Edward Hopper(11), James McNeill Whistler(8), Thomas Eakins(7), John Singer Sargent(2), Arkhip Kuindzhi(1)
49	36	0.69	Early Renaissance	Andrea Mantegna(17), Sandro Botticelli(7), Raffaello Sanzio(6), Jan van Eyck(3), Hieronymus Bosch(2)
37	36	0.50	Spanish Baroque	Bartolomé Esteban Murillo(18), Peter Paul Rubens(6), Titian(4), Frederic Leighton(3), Gustave Doré(2)
4	31	0.48	Persian miniature	Kamāl ud-Dīn Behzād(15), Ustad Mansur(12), Raja Ravi Varma(2), Arcimboldo(1), Kitagawa Utamaro(1)
28	30	0.27	American Realism	Henry Ossawa Tanner(4), Hieronymus Bosch(4), Thomas Eakins(4), Jan van Eyck(3), Sandro Botticelli(3)
21	30	0.57	Ming-dynasty China	Shen Zhou(17), Kawanabe Kyōsai(4), Hasegawa Tōhaku(3), Itō Jakuchū(2), Caspar David Friedrich(1)

Table 16: Top-12 non-noise HDBSCAN clusters on UMAP-20D, sorted by size. Purity is the fraction of points whose movement label matches the cluster’s majority movement. Cluster 21 is the East-Asian cluster combining Shen Zhou, Hasegawa Tōhaku, Kawanabe Kyōsai and Itō Jakuchū; Cluster 41 is the Dutch Golden Age into Spanish Baroque cluster combining Vermeer, Velázquez, Zurbarán, Murillo and Georges de La Tour, the artists most of whose pairs §4 flagged as low-discrimination.

where the pipeline correctly identifies the landscape-painting family as a single stylistic group but makes no attempt to separate the individual artists within it. The limit on artist-level discrimination is in CSD’s output itself, not in the post-processing applied on top of it.

**Verification on UMAP-projected features.** Tab. 17 reports the verification AUCs under manifold-projected features. Numbers are on a single fixed reference split rather than the 25-split mean of main-text Tab. 4, which explains why the cosine-on-raw baseline reads 0.906 here. UMAP-20D drops cosine to 0.795 and pair-logreg to 0.792. UMAP-50D is no better. Concatenating raw and UMAP-projected features does not help over the raw vector alone.

## D T2I evaluation: bare-prompt tier classification and pretest notes

**Bare-prompt tier-classification (full table).** §8 reports three regimes for bare-Flux artist recognition; Tab. 18 gives the full per-artist counts out of the 66 generations per artist (22 neutral subjects  $\times$  3 seeds, prompted as "<subject>, art by <artist>").

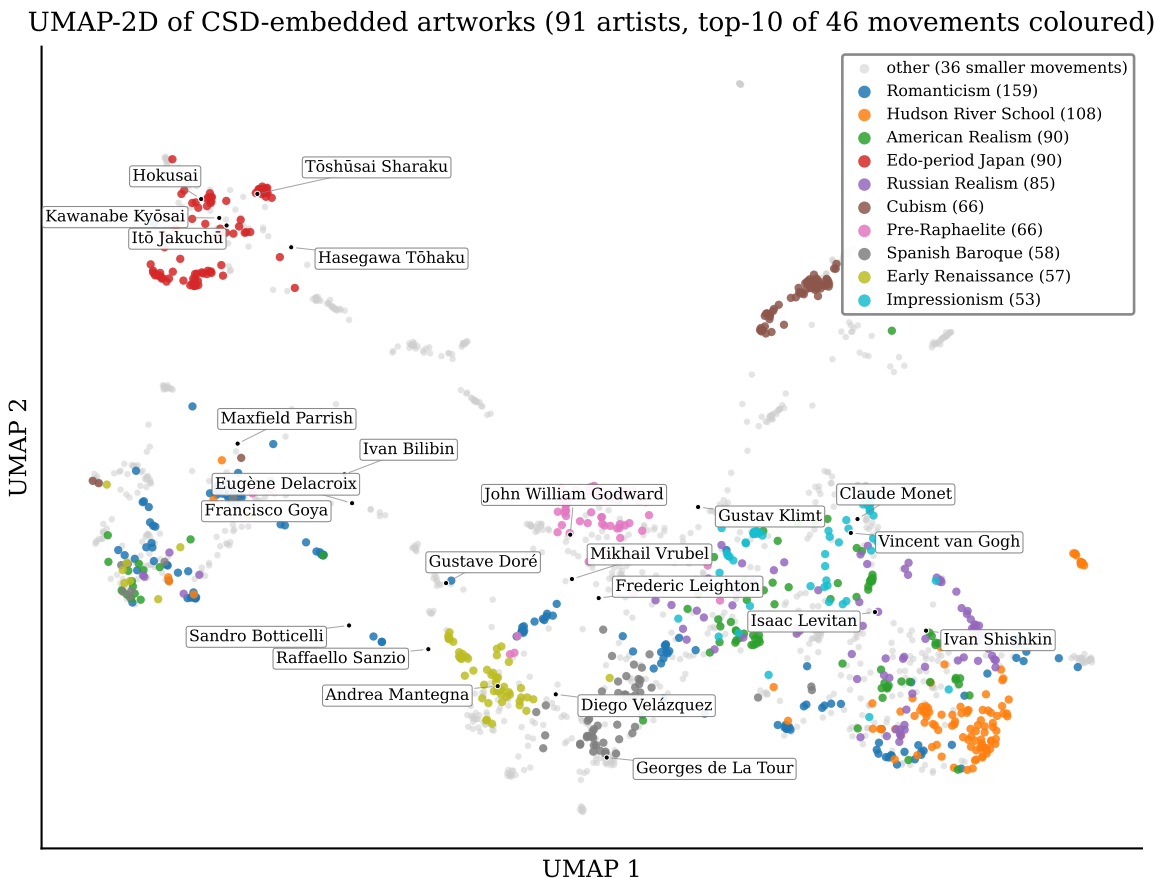


Figure 6: Two-dimensional UMAP projection of the 91-artist corpus. Each point is one anchor, coloured by its primary art-movement / tradition label (47-label author-curated vocabulary); for legibility only the ten largest movements get their own colour, the remaining 37 smaller movements share a neutral grey. Black dots with name boxes mark the artist-level centroids of the worst-gap artists from main-text Tab. 1 together with their pair partners discussed in §4. The 2D projection underestimates separation between clusters that are clean in the 20-dimensional space the actual clustering operates on, so two clusters that appear visually overlapping here may be cleanly separated in 20D; quantitative claims should be read off Tab. 16 above.

**Full LoRA stress-test table.** Tab. 19 expands the compact Tab. 6 of §8 with all (pair, condition, artist) cells across the three negative-gap pairs and two positive-control artists, and reports Bidir(cos), Bidir(CSLs) and Top-1 across all 91 classes for every cell. The positive members of the negative-gap pairs (Sharaku, Godward, Shishkin) are included here for completeness; in the main-text table they are dropped because their bidir is trivially 100% in every condition.

**LoRA fidelity exemplars.** The negative top-1 and bidir numbers in the main table can mislead into reading the trained LoRAs themselves as poor style imitators; they are not. Fig. 7 shows four LoRA outputs spanning four traditions (Edo woodblock print, French Impressionism, Russian Realist landscape, Japanese *kachō-ga*). We deliberately do *not* place authentic anchors next to each generation: the anchors are public-domain scans with age-related patina (yellowed paper, darkened varnish, faded pigment) that the LoRA does not attempt to reproduce, and the side-by-side comparison would unfairly penalise the generations on a dimension orthogonal to style. Read as a gallery, the LoRAs visibly carry the style-defining properties (palette, composition, brushwork, line economy) of the trained artist; what the bidir column of main-text Tab. 6 measures is therefore not training quality but corpus-internal discriminability under raw cosine, the phenomenon §§4/8 are about.

**Caption-template robustness pretest (Sharaku/Kyōsai).** Before the main LoRA stress test we verified that the 100%/0% pair-discrimination asymmetry on the negative-gap pilot pair (§8) is not an artefact of the caption template. On the same trained adapters we generated 30 images per artist with two templates: the full template "late-Edo



(a) Flux-LoRA, Tōshūsai Sharaku style



(b) Flux-LoRA, C. Monet style



(c) Flux-LoRA, I. Levitan style



(d) Flux-LoRA, K. Kyōsai style

Figure 7: LoRA-fidelity exemplars: four Flux-LoRA generations spanning Edo woodblock print, French Impressionism, Russian Realist landscape and Japanese *kachō-ga*, prompt-conditioned on rendered captions of authentic strict-clean anchors. None of these images is a work of the named artist; each is a generation by Flux-1 dev with a per-artist LoRA adapter. Style-defining properties (palette, composition, brushwork, line economy) of the trained artist are visibly carried into the generation; despite the low bidir scores on raw cosine (main-text Tab. 6), the LoRAs themselves are not poor imitators. The discrimination loss is a corpus-internal property of raw cosine, addressed by the diagnostic of §4 and the CSLS readout of §5.

Method	AUC	EER	recall @ $p=0.95$
Pair-logreg on raw CSD-768D	0.927	0.153	0.587
Pair-logreg on concat[raw 768D, UMAP-20D]	0.908	0.177	0.481
Cosine on raw CSD-768D	0.906	0.182	0.561
Cosine on UMAP-20D	0.795	0.283	0.019
Pair-logreg on UMAP-20D only	0.792	0.278	0.001
Pair-logreg on UMAP-50D only	0.785	0.280	0.039
Cosine on UMAP-50D	0.784	0.287	0.103

Table 17: Verification with manifold-projected features. UMAP is fit on the 73 training artists only; the 18 test artists are projected via `umap.transform()`. Numbers are on a single fixed reference split (not the 25-split mean of main-text Tab. 4). Manifold projection drops verification AUC by 0.11 (cosine) and 0.14 (pair-logreg), confirming that UMAP collapses individual-artist discrimination in service of stylistic-family compactness.

Tier	Artist	Top-1 / 66	Top-5 / 66
1 (trigger works)	Tōshūsai Sharaku	37 (56%)	66 (100%)
	Georges de La Tour	35 (53%)	40 (61%)
2 (tradition, not artist)	Frederic Edwin Church	17 (26%)	58 (88%)
	Itō Jakuchū	7 (11%)	49 (74%)
	Sanford R. Gifford	7 (11%)	44 (67%)
	Ivan Shishkin	5 (8%)	28 (42%)
	John W. Godward	2 (3%)	16 (24%)
	Hokusai	0 (0%)	9 (14%)
3 (misses)	Vincent van Gogh	1 (2%)	14 (21%)
	Diego Velázquez	0 (0%)	1 (2%)
	Claude Monet	0 (0%)	1 (2%)
	Gustav Klimt	0 (0%)	0 (0%)
	Frederic Leighton	0 (0%)	0 (0%)
	Isaac Levitan	0 (0%)	0 (0%)

Table 18: Bare Flux-1 dev recognition test. For each prompted artist, the number of generations whose top-1 (and top-5) CSD match in the 91-class strict-clean corpus is the prompted artist. Embedding pipeline: pos-interp 336 (the operational §5 recipe). Tier-1 (trigger works, top-1  $\geq 50\%$ ), Tier-2 (tradition reached, top-1  $< 50\%$  but top-5 substantial), Tier-3 (miss, top-5 below 25%).

Japanese ukiyo-e woodblock print, <trigger>, <subject>" and a stripped variant "woodblock print, <trigger>, <subject>". The full template raises absolute self-cosines (Sharaku 0.308  $\rightarrow$  0.503, Kyōsai 0.225  $\rightarrow$  0.370), but pair-bidirectional discrimination is identical: Sharaku reaches 100% and Kyōsai 0% in both. The asymmetry is therefore a property of the CSD geometry, not of the inference prompt.

## E Reproducibility

**Software and precision.** The CSD ViT-L/14 checkpoint is the one released by Somepalli et al. [14], used without modification at the standard  $224 \times 224$  input. Pos-interp inference uses bilinear interpolation of the trained positional embeddings to a  $24 \times 24$  grid for  $336 \times 336$  input. DINOv2-Large [8] is used in its public pretrained configuration. All embedding computations are performed in fp32; results are deterministic given the random seeds reported below. Clustering uses UMAP, HDBSCAN, scikit-learn (PCA, random projection, NMF, average-linkage agglomerative, Ward,  $k$ -means) and `leidenalg` for Leiden community detection. Verification trains logistic regression and Cholesky-parametrised Mahalanobis on the 73 training artists and tests on the 18 held-out artists across 25 random seed-controlled splits. The full analysis pipeline runs on a single GPU; no multi-GPU configuration is required.

**Random seeds.** The 25 verification splits are drawn from a fixed seed family  $\{0, 1, \dots, 24\}$ . UMAP and Leiden experiments report mean  $\pm$  standard deviation across seeds  $\{0, \dots, 9\}$  where stated. Every result reported as "25/25" refers to a paired comparison across the 25 verification splits where the recipe in question wins on every split against the cosine-on-raw baseline.

Pair	Cond.	Artist	N	Bidir(cos)	Bidir(CSLS)	Top-1(91)
Edo (gap $-0.049$ )	bare	Tōshūsai Sharaku	66	66/66 (100%)	38/66 (58%)	43/66 (65%)
Edo (gap $-0.049$ )	bare	Kawanabe Kyōsai	66	0/66 (0%)	36/66 (55%)	0/66 (0%)
Edo (gap $-0.049$ )	lora	Tōshūsai Sharaku	69	69/69 (100%)	69/69 (100%)	69/69 (100%)
Edo (gap $-0.049$ )	lora	Kawanabe Kyōsai	60	7/60 (12%)	47/60 (78%)	0/60 (0%)
Victorian (gap $-0.039$ )	bare	Frederic Leighton	66	1/66 (2%)	3/66 (5%)	0/66 (0%)
Victorian (gap $-0.039$ )	bare	John W. Godward	66	66/66 (100%)	63/66 (95%)	4/66 (6%)
Victorian (gap $-0.039$ )	lora	Frederic Leighton	57	0/57 (0%)	3/57 (5%)	0/57 (0%)
Victorian (gap $-0.039$ )	lora	John W. Godward	75	75/75 (100%)	75/75 (100%)	72/75 (96%)
Russian (gap $-0.030$ )	bare	Isaac Levitan	66	0/66 (0%)	0/66 (0%)	0/66 (0%)
Russian (gap $-0.030$ )	bare	Ivan Shishkin	66	66/66 (100%)	66/66 (100%)	7/66 (11%)
Russian (gap $-0.030$ )	lora	Isaac Levitan	60	5/60 (8%)	6/60 (10%)	0/60 (0%)
Russian (gap $-0.030$ )	lora	Ivan Shishkin	63	63/63 (100%)	63/63 (100%)	40/63 (63%)
Tier-3 control	bare	Claude Monet	66	—	—	0/66 (0%)
Tier-3 control	lora	Claude Monet	48	—	—	7/48 (15%)
Tier-2 control	bare	Hokusai	66	—	—	0/66 (0%)
Tier-2 control	lora	Hokusai	39	—	—	3/39 (8%)

Table 19: Full LoRA stress test: every (pair, condition, artist) cell with all three readouts. Bidir(cos) and Bidir(CSLS) measure pair-bidirectional discrimination against strict-clean anchors; Top-1(91) is top-1 match in the 91-class corpus. The bare-Flux Bidir(CSLS) values for the negative pair members (55–95%) are an artefact of CSLS on the bare-prompt distribution where many “art by X” generations of one artist still land in  $X$ ’s neighbourhood for unrelated reasons (e.g. subject overlap); they are not a recovery of the negative gap on T2I generations. The LoRA-CSLS column is the operational reading.

**Strict-clean filter.** The strict-clean anchor set used throughout this paper is the output of a single-source-of-truth filter applied to the post-attribution pool: an image is admitted iff its `is_artwork_by_artist` channel is true, its `artwork_kind` is in  $\{painting, drawing, print, watercolour, mixed\_media\}$ , both `has_frame` and `has_museum_context` are false, and its caption does not match a curated set of suspect-caption regular expressions targeting reproductions, postcards, plaques and book covers. Artists with fewer than ten admissible anchors are dropped from the working corpus. The same filter applies uniformly to all backbones and all input pipelines reported in the paper, so cross-backbone and cross-input numbers reference the same 1799-image, 91-artist set; the resulting embedding NPZ files therefore differ only in the embedding function applied to identical input pixels.

**Per-image licence and attribution side-channels.** Each retained anchor carries an attribution label in  $\{master, workshop, school, after, attributed\}$  from the language-model attribution audit and a licence-metadata record captured at fetch time from the corresponding Wikimedia Commons entry. Both side-channels are carried into the embedding NPZ as parallel arrays of length  $N=1799$ , so any downstream analysis can condition on attribution class or licence status without re-fetching.